

Keck Next Generation Adaptive Optics Science Requirements Document

Release 1

November 12, 2006

| | |
|---|----------|
| EXECUTIVE SUMMARY | 3 |
| 1 INTRODUCTION | 3 |
| 1.1 BACKGROUND | 3 |
| 1.2 JWST AND ALMA CAPABILITIES..... | 4 |
| 2 SCIENCE CASES | 5 |
| 2.1 MULTIPLICITY, SIZE, AND SHAPE OF MINOR PLANETS | 5 |
| 2.1.1 Scientific background and context | 5 |
| 2.1.2 Scientific goals..... | 5 |
| 2.1.3 Proposed observations and targets..... | 5 |
| 2.1.3.1 Size and shape..... | 5 |
| 2.1.3.2 Orbits of multiple asteroidal systems | 7 |
| 2.1.4 AO and instrument requirements..... | 9 |
| 2.1.5 Performance Requirements (roll-up of performance requirements) | 9 |
| 2.1.5.1 Wavefront error | 9 |
| 2.1.5.2 Encircled energy | 10 |
| 2.1.5.3 Generalized anisoplanatism | 10 |
| 2.1.5.4 Photometric precision..... | 10 |
| 2.1.5.5 Astrometric precision | 10 |
| 2.1.5.6 Contrast | 10 |
| 2.1.5.7 Polarimetric precision | 11 |
| 2.1.5.8 Backgrounds | 11 |
| 2.1.5.9 Overall transmission..... | 11 |
| 2.1.6 Other key design features..... | 11 |
| 2.1.6.1 Required observing modes..... | 11 |
| 2.1.6.2 Observing efficiency | 11 |
| 2.1.7 Instrument requirements (visible and infrared imager)..... | 12 |
| 2.1.7.1 Field of view | 12 |
| 2.1.7.2 Field of regard..... | 12 |
| 2.1.7.3 IFU multiplicity | 12 |
| 2.1.7.4 Wavelength coverage | 12 |
| 2.1.7.5 Spectral resolution | 12 |
| 2.1.8 References..... | 12 |
| 2.2 IMAGING AND CHARACTERIZATION OF EXTRASOLAR PLANETS AROUND NEARBY STARS..... | 13 |
| 2.2.1 Scientific background and context | 13 |
| 2.2.2 Scientific goals..... | 13 |
| 2.2.2.1 Planets around low-mass stars and brown dwarfs | 14 |
| 2.2.2.2 Very young planets in the nearest star-forming regions | 15 |
| 2.2.3 AO and instrument requirements (for each sub-case)..... | 15 |
| 2.2.4 Performance Requirements | 16 |
| 2.2.4.1 Wavefront error | 16 |
| 2.2.4.2 Encircled energy | 16 |
| 2.2.4.3 Generalized anisoplanatism | 16 |
| 2.2.4.4 Photometric precision..... | 16 |
| 2.2.4.5 Astrometric precision | 16 |

| | | |
|----------|--|-----------|
| 2.2.4.6 | Contrast | 16 |
| 2.2.4.7 | Polarimetric precision | 16 |
| 2.2.4.8 | Backgrounds | 16 |
| 2.2.4.9 | Overall transmission | 17 |
| 2.2.5 | Other key design features | 17 |
| 2.2.5.1 | Required observing modes | 17 |
| 2.2.5.2 | Observing efficiency | 17 |
| 2.2.6 | Instrument requirements | 17 |
| 2.2.6.1 | Field of view | 17 |
| 2.2.6.2 | Field of regard | 17 |
| 2.2.6.3 | IFU multiplicity | 17 |
| 2.2.6.4 | Wavelength coverage | 17 |
| 2.2.6.5 | Spectral resolution | 17 |
| 2.2.7 | References | 17 |
| 2.3 | PRECISION ASTROMETRY: MEASUREMENTS OF GENERAL RELATIVITY EFFECTS IN THE GALACTIC CENTER | 18 |
| 2.3.1 | Scientific background and goals | 18 |
| 2.3.2 | General Relativistic Effects | 18 |
| 2.3.3 | R_0 and the dark matter halo | 20 |
| 2.3.4 | Proposed observations and targets | 21 |
| 2.3.5 | Observing plan for Astrometric Imaging: | 21 |
| 2.3.6 | Observing plan for Radial Velocity Measurements (IFU spectroscopy): | 22 |
| 2.3.7 | Current issues and limitations that could be further explored with existing data sets | 22 |
| 2.3.8 | AO requirements | 23 |
| 2.3.9 | General comments on astrometric accuracy in an AO system with multiple deformable mirrors | 23 |
| 2.3.10 | Radial Velocity: | 24 |
| 2.3.11 | Instrument requirements | 25 |
| 2.3.12 | References | 25 |
| 2.4 | RESOLVED STELLAR POPULATIONS IN NEARBY GALAXIES | 27 |
| 2.5 | GALAXY ASSEMBLY AND STAR FORMATION HISTORY | 28 |
| 2.5.1 | Introduction | 28 |
| 2.5.2 | Scientific background and context: galaxies at $2 \leq z \leq 3$ | 28 |
| 2.5.3 | Scientific goals | 29 |
| 2.5.4 | Proposed observations and targets | 30 |
| 2.5.5 | AO and instrument requirements | 31 |
| 2.5.5.1 | AO Requirements | 32 |
| 2.5.5.2 | Instrument Requirements: | 33 |
| 2.5.6 | References | 33 |
| 3 | APPENDIX A. TABLE OF POTENTIAL INFRARED TIP-TILT STARS CLOSE TO THE GALACTIC CENTER | 35 |

Executive Summary

To be written

1 Introduction

1.1 Background

The Science Team of the Keck NGAO project is charged with 1) identifying the science requirements for the Next-Generation Adaptive Optics (NGAO) system, and 2) when design trade-offs must be made, ensuring that the NGAO system will be built with capabilities that enable the key science cases to the greatest extent possible.

This document, which will be referred to as the Science Requirements Document (SRD), is a “living document”, and will be updated as the science case is developed with increasing fidelity. Initially, the SRD will rely on and heavily reference the science cases developed for the Proposal to the Keck Science Steering Committee prepared in June 2006. Key issues are (a) the importance of the science enabled by the AO system and its accompanying instruments; (b) the advances offered by NGAO relative to AO systems being developed on other telescopes (discovery space); and (c) complementarity to the James Webb Space Telescope (JWST) and the Atacama Large Millimeter Array (ALMA), which will be commissioned on the same timescale as Keck NGAO will be commissioned.

Since June 2006, the Project Scientist has met with subgroups of the Science Team in order to re-examine the science cases, to develop more solid requirements, and to look in more detail at the associated Instrument and Observatory requirements. This document, Release 1 of the SRD, describes AO and instrument requirements for a subset of NGAO science that is anticipated to have impact on the following AO system error budgets and instrument requirements:

- AO and instrument background requirements
- wavefront error
- astrometric error budget
- field of view and field of regard
- spectral resolution and multiplicity for the deployable integral field unit instrument
- AO capabilities at visible wavelengths

1.2 JWST and ALMA Capabilities

JWST is a cryogenic 6.5m space telescope expected to be launched in 2013, and will have considerably higher faint-source sensitivity than Keck NGAO due to its low backgrounds. Its NIRCAM instrument will image in 14 filters in the 0.6-2.3 μm wavelength range that overlaps with Keck NGAO. NIRCAM will have a 2.2 x 2.2 arc-minute field of view, a pixel scale of 0.035 arc sec for 0.6-2.3 μm wavelengths, and coronagraphic capability. NIRCAM has diffraction-limited imaging for wavelengths between 2.4 and 5 μm , but not below 2 μm due both to the primary mirror quality specification and to the pixel scale (0.035 arcsec) within NIRCAM. NIRSpec is a near infrared multi-object dispersive spectrograph for JWST in the 0.6 - 5 μm band. The NIRSpec design provides 3 observing modes: a low resolution $R\sim 100$ prism mode, an $R\sim 1000$ multi-object mode, and an $R\sim 3000$ mode. In the $R\sim 100$ and $R\sim 1000$ modes NIRSpec provides the ability to obtain simultaneous spectra of more than 100 objects in the 3.4 x 3.4 arcmin field of view. Spatial pixel size will be 0.1 arc sec. There will be an integral field spectrograph with field of view 3" x 3". (It is not clear from recent documentation whether the spectral resolution for the IFU will be $R=1000$ or 3000. We need to find out.) The primary goal for NIRSpec is enabling large surveys of faint galaxies ($1 < z < 5$) and determining their metallicity, star formation rate, and reddening.

ALMA is a powerful new facility for mm and sub-mm astrophysics that is currently scheduled to begin science operations in 2012. It will consist of 54 12-m and 12 7-m antennas located at an altitude of 5000m (16,500 feet) in the Atacama desert of Chile. ALMA will observe, with very high sensitivity and resolution, the cold regions of the Universe, which are optically dark, yet shine brightly in the millimeter portion of the electromagnetic spectrum. With a baseline that is controllable from 150 m to 18 km, it will have spatial resolution down to 0.01 arc-seconds (0.004 arc-seconds at the highest frequencies), with typical spatial resolution of 0.1 arc-second or better. It is expected to operate within atmospheric windows from 0.35 to 9 mm. Among other things, it will excel at the study of chemical evolution in star-forming regions at $z \sim 3$, dust-gas interactions, molecules surrounding stars, and molecular clouds. With its great sensitivity it will detect dust emission out to $z=20$. It will reveal the kinematics of obscured galactic nuclei and quasi-stellar objects on spatial scales smaller than 100 pc.

2 Science Cases

2.1 Multiplicity, Size, and Shape of Minor Planets

Author: Franck Marchis

Editor: Claire Max

2.1.1 Scientific background and context

While space missions largely drove early progress in planetary astronomy, we are now in an era where ground-based telescopes have greatly expanded the study of planets, planetary satellites and the asteroid and Kuiper belts. Ground-based telescopes can efficiently perform the regular observations needed for the monitoring of planetary atmospheres and geology, and ground-based telescopes can quickly respond to transient events.

The study of the remnants from the formation of our solar system provides insight into the proto-planetary conditions that existed at the time of formation. Such information has been locked into the orbits and properties of asteroids and Kuiper Belt objects. The study of binary (and multiple) minor planets is one key path to revealing these insights, specifically by studying their kinematics and geological properties. However, there are no space missions currently planned to study these binaries. This important line of inquiry is only accessible to ground-based telescopes equipped with AO.

2.1.2 Scientific goals

High angular resolution studies are needed of large samples of binaries to understand how their enormous present-day diversity arose from their formation conditions and subsequent physical evolution, through processes such as disruption and re-accretion, fragmentation, capture ejecta, fission among others.

- Formation and interior of minor planets by accurate estimate of the size and shape of minor planets and its companion.
- Mass, density, distribution of material in the interior by a precise determination of the orbital parameters of the moonlet satellites
- Chemical composition and age of the system combining high angular resolution with spectroscopic analysis (briefly mentioned in this document in the instrument requirement)

2.1.3 Proposed observations and targets

2.1.3.1 Size and shape

Spatially resolved imaging of other large asteroids is critical in order to place the results for Vesta into context and to derive truly reliable statistical constraints on

large collisions throughout the Main Belt. Observations of the 15 or 20 largest asteroids would provide the statistics necessary to put much stronger constraints on the frequency of these large collisions. We estimate that 20 Main Belt asteroids will be resolved with sufficient resolution with NGAO in R-band (33 in V-band) for mapping comparable to that done previously for 4 Vesta.

Table 1 summarizes the number of asteroids resolvable from visible to near-IR domain and per population. Thanks to the high angular resolution provided in V and R bands, ~800 main-belt asteroids could be resolved and have their shape estimate with a precision of less than 7%. With current AO system ~100 asteroids, located only in the main-belt, can be resolved. The determination of the size and shape of Trojan asteroids, even if limited to a few of them, will be useful to estimate their albedo. For NEAs, the large number of resolvable objects is a result of very close approaches to Earth.

Table 1 Number of Asteroids resolvable with Keck NGAO in various wavelength ranges and populations

| Resolvable asteroids in each band (numbered and unnumbered) | | | | | | |
|--|----------|----------|----------|----------|----------|----------|
| Orbital type | V | R | I | J | H | K |
| Near Earth | 526 | 460 | 376 | 269 | 204 | 152 |
| Main Belt | 855 | 716 | 526 | 319 | 194 | 100 |
| Trojan | 13 | 11 | 5 | 0 | 0 | 0 |
| Centaur | 1 | 1 | 1 | 0 | 0 | 0 |
| TNO | 3 | 3 | 3 | 3 | 3 | 3 |
| Other | 4 | 2 | 1 | 0 | 0 | 0 |

However, this research program will have a higher impact if it is combined with the study of binary asteroids. Recent studies suggested that primary asteroid of most binary asteroid systems has a rubble-pile structure, indicating that they have a weak shear strength (Marchis et al., 2006). Consequently their shape is directly related to the angular momentum at their formation (Tanga et al., 2006). One can obtain their mass through determination of the moonlet orbit, combined with a good shape estimate by direct observations in the visible (which provides the best angular resolution). We estimate that between 1000-4000 binary asteroids could be discovered with NGAO. An accurate shape estimate for ~300 of them (1 order of magnitude more than the current known shapes for asteroids) can be easily attainable with NGAO in visible. A SNR of 1000-3000 of these 7-16 magnitude targets can be reached in 5 min of integration time. Six observations taken at various longitudes are enough to accurately reconstruct the 3D-shape of the asteroid. Twelve nights of observations should be considered for the completion of such a program. Dedicated nights are not necessary since this program can be combined with the study of satellite orbits of asteroids (same instrumentation)

2.1.3.2 Orbits of multiple asteroidal systems

Study of main-belt multiple systems: One of the main limitations of current AO observations for a large search of binary asteroid and characterization of their orbit is the limited quantity amount of asteroids observable considering the magnitude limit on the wavefront sensor. The Keck NGS AO system reaches a 13.5 magnitude, so ~ 1000 main-belt asteroids (to perihelion >2.15 AU and aphelion <3.3 AU) can be observed.

With NGAO providing an excellent correction up to tip-tilt star magnitude 17, 10% of the known main-belt population can be scanned, corresponding to the potential discovery of 1000-4000 multiple systems. Additionally because the NGAO system will provide a better and more stable correction (compared to the Keck LGS AO), the halo due to uncorrected phase errors will be significantly reduced.

Closer and fainter satellites should be detectable; therefore we will be able to detect more multiple asteroid systems. More close binary systems could be also characterized because of the better angular resolution provided in the visible wavelength range (FWHM ~ 14 mas in R band). At the time of writing, the orbits of ~ 13 visual binary systems are known and display considerable diversity. To better understand these differences, we propose to focus our study on 100 new binary systems in the main-belt discovered by lightcurve or snap shot programs on HST and/or previous AO systems. The increase by an order of magnitude of known orbits will help to how they formed considering, for instance, the asteroids as members of acollisional family, their distance to the Sun, their size and shape, and other parameters.

To reach a peak SNR ~ 1000 -3000 on an AO image, the typical total integration times for 13th or 17th magnitude targets are 5 min and 15 min respectively. Considering a current overhead of 25 min (Marchis et al. 2004b) to move the telescope onto the target and close the AO loop, the total telescope time per observation is ~ 30 min. (This overhead time should be significantly improved by careful design of the NGAO system.) The orbit of an asteroid can be approximated (P, a, e, i) after 8 consecutive observations (taken over a period of 1-2 months to limit the parallax effect), corresponding to the need for 0.3 nights per object. Thirty nights of observation would be requested for this program over 3 years.

To illustrate the gain in quality expected with NGAO, we generated a set of simulated images of the triple asteroid system 87 Sylvia. The binary nature of this asteroid was discovered in 2001 using the Keck NGS AO system. Marchis et al. (2005c) announced recently the discovery of a smaller and closer moonlet. The system is composed of a $D=280$ km ellipsoidal primary around which two moons describe a circular and coplanar orbit: "Romulus", the outermost moonlet ($D=18$ km) at 1356 km ($\sim 0.7''$) and "Remus" ($D = 7$ km) at 706 km ($\sim 0.35''$). In our simulation we added artificially two additional moonlets around the primary: "S1/New" ($D=3.5$ km) located between Romulus and Remus (at 1050 km) and "S2/New" ($D=12$ km) closer to the primary (at 480 km). This system is particularly difficult to observe

since the orbits of the moons are nearly edge-on. We blurred the image using the simulated NGAO and Keck NGS AO PSFs (with an rms error of 140 nm) and added Poisson and detector noise to reach a S/N of 2000 (corresponding to 1-3 min integration time for a 12th visible magnitude target). We then estimated whether the moonlets could be detected and their intensity measured by aperture photometry. Figure 1 displays a comparison for one observation between the Keck NGS AO, NGAO in two wavelengths, and HST/ACS. The angular resolution and thus the sensitivity of the NGAO R-band is a clear improvement and permits detection of the faintest moon of the system.

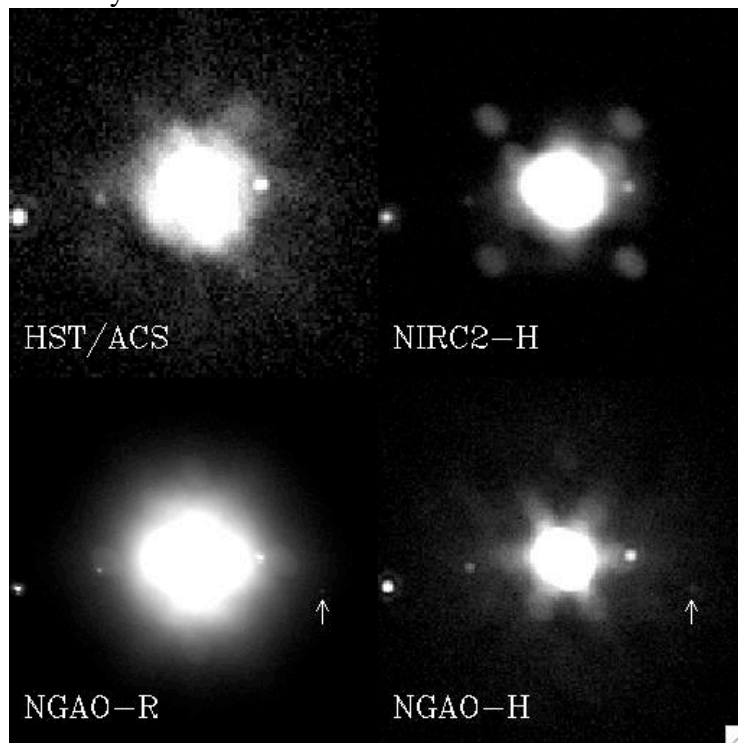


Figure 1. Simulation of pseudo-Sylvia observed with various AO systems

Table 2 summarizes the detection rate for the pseudo-Sylvia system moonlets. The photometry was done using the same technique as for real observations (aperture photometry + fitting/correction of flux lost). The detection rates for NGAO- R band are 100% for all moons. One can also notice a very good photometric recovery with this AO system. The chances to discover multiple systems and to analyze them are significantly improved with NGAO. It should be also emphasized that because the astrometric accuracy is also better, determination of the orbital elements of the moons will be also more accurate (e.g., a significant eccentricity or small tilt of the orbit).

Table 2 **Detection rate and photometry on the moons of pseudo-Sylvia.**
(with various AO systems and wavelength of observations).

| | Romulus | | Remus | | S_New1 | | S_New2 | |
|----------------------|-----------|------------|-----------|------------|-----------|------------|-----------|------------|
| | Det. rate | Δm |
| Perfect image | 100% | 6.6 | 100% | 8.1 | 100% | 6.9 | 100% | 9.6 |
| NIRC2-H | 82% | 6.4±0.04 | 70% | 8.3±0.3 | 11% | 6.9±0.2 | 0% | N/A |
| NGAO-H | 100% | 7.0±0.1 | 70% | 8.5±0.5 | 40% | 7.1±0.2 | 0% | N/A |
| NGAO-R | 100% | 6.60±0.01 | 100% | 8.3±0.1 | 100% | 6.9±1.1 | 100% | 10.1±0.3 |

2.1.4 AO and instrument requirements

Note: need to do comparisons of the science that can be done at 140nm versus 170nm and higher. The initial 140nm figure used below was taken from the Proposal to the SSC, June 2006.

Size and Shape:

An AO system providing a good on-axis correction (WF error of 140 nm) and a visible camera with at least Nyquist sampling is the most interesting instrument for this science case.

Orbit determination:

This observing program requires imaging capabilities. An on-axis AO system (with WFE~140 nm) will also characterize a large number of known main-belt binary systems in more physical detail than is known today.

A visible imager is our first priority since more multiple asteroidal systems could be studied thanks to a better angular resolution. In addition, visible light should provide more precise astrometric and photometric accuracy. *Note: this needs to be checked.* A NIR imager would be useful for the specific case of multiple TNOs.

2.1.5 Performance Requirements (roll-up of performance requirements)

2.1.5.1 Wavefront error

Note: need to repeat simulations for WF errors higher than 140nm, in order to see where the science starts to really suffer.

A WF error of 140 nm will provide excellent angular resolution in visible, better than HST and adequate for our program. We expect excellent sensitivity for point source detection. Table 14 of the Keck NGAO Proposal to the SSC (June 2006) indicates that the point source limiting magnitude for such AO system (5s, 1hr integration) is 29.0 in R band. For comparison, recent observations of Pluto-Charon recorded with ACS/WFC at 0.61 μm (Weaver et al., 2006), allowed the detection of

2 new moons with $R = 23.4$ ($\text{SNR}=35$). With NGAO in R band with 140 nm of wavefront error, these moons could have been discovered with $\text{SNR}\sim 47$. Such gain in sensitivity will help find more multiple systems, and also to find out if around these multiple systems there is still a ring of dust left over from the catastrophic collision that formed the multiple system. **Question: what observing requirements and instruments would be needed to detect the dust?**

2.1.5.2 Encircled energy

N/A

2.1.5.3 Generalized anisoplanatism

FOV is 2" so anisoplanetic effects are negligible.

2.1.5.4 Photometric precision

Accurate photometry will lead to a better estimate of the size and shape of the moonlet, which will give strong constraint on the formation of the system (e.g. if the moon is synchronized and displays an equilibrium shape formed by tidal effects). With current AO systems, the photometric accuracy on the moonlet is quite poor due to the imperfection of the AO. The accuracy of the flux estimate of the 22 Kalliope moonlet, orbiting at 0.6" with $\Delta m=3$, is $\sim 20\%$. **With NGAO in the NIR, the photometry accuracy for the same body should be at least 5% (need more precise calculations here... backgrounds and visible wavelengths need to be considered)**

2.1.5.5 Astrometric precision

The astrometric measurements for our program are relative to the primary. The maximum angular separation between the secondary and the primary is 0.7". We require the visible instrument to provide images with at least Nyquist sampling: a pixel scale of 6 mas is needed. The relative position of the secondary, estimated by a Moffat-Gauss fit, cannot be better than a 1/4 of pixels (since the primary is resolved). The residual distortion on the 2" FOV of the detector should not be more than 1.5 mas. **Note: need to think about achievable astrometric accuracy as a function of how bright the main asteroid and moonlets are.**

2.1.5.6 Contrast

At the time of writing the faintest and closest moonlet discovered around an asteroid is Remus, orbiting at 0.2-0.5" (350-700 km) around 87 Sylvia with Δm (peak-to-peak) = 3.5. The detection of this moonlet is challenging with current Keck AO, and also with the VLT NACO system. For instance, it was detected ($\text{SNR}>3$) on 10 images out of 34 recorded over 2 months with the VLT. A better contrast will increase the detection rate, allowing us to see fainter and closer moonlets for instance, but also to get a better photometric measurement on those already known. Coronagraphic observations cannot be considered in our case, since the central source is not point-like so the effect of the mask will be negligible. It is assumed that the distance to the primary of a satellite is driven by tidal effects, but at the moment

theoretical work fails to agree on the age of an asteroid and the position of its moonlet. This is mostly due to the lack of observational systems into which a moonlet orbits at less than 1000 km ($a / R_p < 8$). Two orders of magnitude gain in the detection limit ($\Delta m = 5.5$ at $0.5''$) will lead to the possibility of detecting a half-size moonlet around (87) Sylvia.

2.1.5.7 Polarimetric precision

N/A

2.1.5.8 Backgrounds

N/A (visible)

2.1.5.9 Overall transmission

This need further work. The calculations below assume the same overall transmission as Keck AO or VLT/NACO

2.1.6 Other key design features

2.1.6.1 Required observing modes

The capability of efficiently observing moving targets must be included in the design of NGAO, so that implementation of differential guiding when the tip-tilt source is not the object itself (and is moving relatively to the target) is possible.

We also point out that for this science case, the scientific return of the Keck telescope and the NGAO system will greatly improve if service observing (i.e., queue scheduling) is offered. With an error budget of 140 nm the NGAO system will achieve a SR of $\sim 20\%$ in R- band under moderate seeing conditions. Bright targets like the Galilean satellites ($V \sim 6$) can be observed even if the seeing conditions are lower than average in the NIR ($> 1.2''$). Other difficult observations, such as the study of multiple TNOs ($V > 17$) could be scheduled when the seeing conditions are excellent ($< 0.7''$). Finally, frequent and extremely short (half hour) direct imaging observations of a specific target such as Io, to monitor its activity over a long period of time, would be extremely valuable and are not available on HST. All these programs could be done more easily if service observing were available at Keck. It would also drastically relax the constraints on the NGAO error budget since it would be possible to take advantage of excellent atmospheric conditions to observe the fainter objects.

2.1.6.2 Observing efficiency

Current observations with Keck AO have a ~ 25 minute overhead when switching between targets for an on-axis LGS observation. It is very desirable to reduce this overhead. A goal of 10 minutes setup time when switching between LGS targets is desirable. There is no firm requirement, but observing efficiency suffers in direct proportion to the time it takes to switch from one target to the next, particularly

when the observing time per target is relatively short. This is an important constraint for this science case, since numerous targets must be observed per night.

2.1.7 Instrument requirements (visible and infrared imager)

2.1.7.1 Field of view

No more than 2". On-axis observing. (Density of asteroids on the sky is not high enough for multi-object observing.)

2.1.7.2 Field of regard

Should be determined by the requirement to find adequate tip-tilt stars.

2.1.7.3 IFU multiplicity

N/A

2.1.7.4 Wavelength coverage

0.7 – 2.5 μm for imaging.

2.1.7.5 Spectral resolution

This spec needs more work. There are spectroscopic features at visible wavelengths (e.g. the absorption bands of pyroxene between 0.85 - 1 μm). Need to prioritize these and think about required spectral resolution (bands are broad).

R~400 in visible

R~1000 in NIR

2.1.8 References

To be DONE

2.2 Imaging and characterization of extrasolar planets around nearby stars

Author: Michael Liu

Editor: Claire Max

2.2.1 Scientific background and context

The unique combination of high-contrast near-IR imaging (K-band Strehl ratios of 80-90%) and large sky coverage delivered by NGAO will enable direct imaging searches for Jovian-mass planets around nearby young low-mass stars and brown dwarfs. Both the Gemini Observatory and ESO are developing highly specialized planet-finding AO systems with extremely high contrast for direct imaging of young planets. These "extreme AO" systems are very powerful, but their design inevitably restricts them to searches around bright, solar-type stars ($I=8$ to 9 mag).

NGAO will strongly distinguish work at WMKO from all other direct imaging searches planned for large ground-based telescopes. By number, low-mass stars ($M \leq 0.5 M_{\text{Sun}}$) and brown dwarfs dominate any volume-limited sample, and thus these objects may represent the most common hosts of planetary systems. Such cool, optically faint targets will be unobservable with specialized extreme AO systems because their parent stars are not bright enough to provide a high-order wavefront reference. But thousands of cool stars in the solar neighborhood can be targeted by NGAO. Direct imaging of extrasolar planets is substantially easier around these lower mass primaries, since the required contrast ratios are smaller for a given companion mass.

2.2.2 Scientific goals

Direct imaging of extrasolar planets by NGAO would allow us to measure their colors, temperatures, and luminosities, thereby testing theoretical models of planetary evolution and atmospheres. NGAO spectroscopic follow-up will be an important means to characterize the atmospheres of extrasolar planets, which are otherwise essentially inaccessible to spectroscopy. Figure 1 (need to fix figure numbers) summarizes the relative parameter space explored by NGAO and extreme AO. The complementarity of the two systems is very important: establishing the mass and separation distribution of planets around a wide range of stellar host masses and ages is a key avenue to understanding the planet formation process. The optical faintness of low-mass stars, brown dwarfs and the very youngest stars make them inaccessible to extreme AO systems but excellent targets for NGAO.

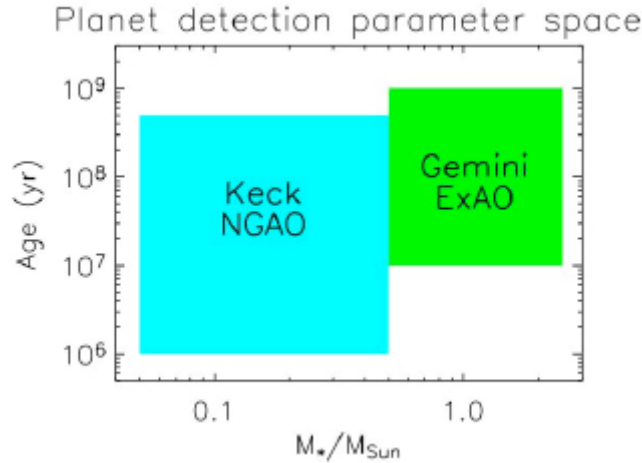


Figure 1: Schematic illustration of the parameter space of NGAO and the Gemini Planet Imager for direct imaging of extrasolar planets.

2.2.2.1 Planets around low-mass stars and brown dwarfs

Direct imaging of substellar companions (brown dwarfs and extrasolar planets) is substantially easier around lower mass primaries, since the required contrast ratios are smaller for a given companion mass. Indeed, the first bona fide L dwarf and T dwarfs were discovered as companions to low-mass stars (Becklin & Zuckerman 1988, Nakajima et al 1995). Thus, searching for low-mass stars and brown dwarfs is an appealing avenue for planet detection and characterization. Given that low-mass stars are so much more abundant than higher mass stars, they might constitute the most common hosts of planetary systems. Figure 2 shows an estimate of the planet detection sensitivity for NGAO.

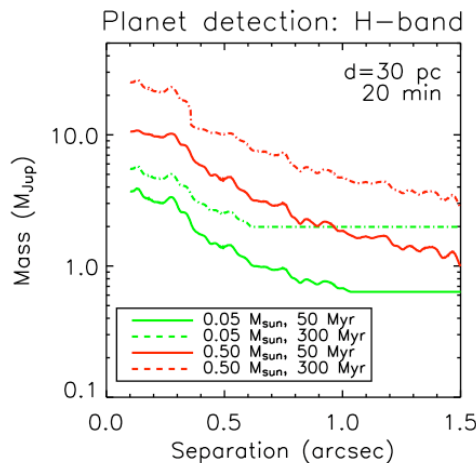


Figure 2: Estimated NGAO sensitivity for direct imaging of planets around low-mass stars (red lines) and brown dwarfs (green lines). **Need to specify wavefront error for these graphs, and compare for several different values of the WFE (e.g. 140, 170, 200 nm).**

NGAO will be able to search for Jovian-mass companions around large numbers of low-mass stars and brown dwarfs in the solar neighborhood

Spectroscopic follow-up of the coldest companions will be an important path in characterizing the atmospheres of objects in the planetary domain. Strong molecular absorption features from water and methane provide diagnostics of temperature and surface gravity at modest ($R \sim 100$) spectral resolution. Below $\sim 500 \text{ K}$, water clouds are expected to form and may mark the onset of a new spectral class, a.k.a. "Y dwarfs". Such objects represent the missing link between the known T dwarfs and Jupiter, but are probably too faint and rare to be detected as free-floating objects in shallow all-sky surveys such as 2MASS and SDSS. Furthermore, the coolest/lowest

mass objects may not exist as free-floating objects if there is a low-mass cutoff to the initial mass function of the star formation process, e.g., from opacity-limited fragmentation of molecular clouds ($M_{\min} \sim 5\text{-}10 M_{\text{Jup}}$; Silk 1977). Even cooler/lower mass objects might only form via fragmentation, akin to the formation of binary stars, and may only be found as companions.

2.2.2.2 Very young planets in the nearest star-forming regions

Imaging searches and characterization at the very youngest (T Tauri) stages of stellar evolution provide a unique probe of the origin of extrasolar planets, by constraining their formation timescales and orbital separations. Young stars and brown dwarfs can be enshrouded by substantial dust extinction, both from the natal molecular cloud and their own circumstellar material. Thus most young (T Tauri) stars are too optically faint for current NGS AO systems or future ExAO systems. Keck NGAO imaging will probe physical separations of $\geq 5\text{-}10$ AU around these stars.

It is still an open question whether giant planets form extremely rapidly ($\leq 10^4$ yr) due to disk instabilities (e.g. Boss 1998) or if they first assemble as $\sim 10 M_{\text{earth}}$ rocky cores and then accrete $\sim 300 M_{\text{earth}}$ of gaseous material over a total timescale of $\sim 1\text{-}10$ Myr (e.g. Lissauer 1999). Potentially both mechanisms may be relevant, depending on the range of orbital separations and circumstellar disk masses. In addition, imaging searches of both young T Tauri stars with disks (classical TTS) and without disks (weak TTS) can help to constrain the formation timescale. In particular, weak T Tauri stars with planetary companions would suggest that planet formation could occur even when disk evolution/dissipation happens rapidly.

2.2.3 AO and instrument requirements (for each sub-case)

The **high contrast near-IR (0.9-2.5 micron) imaging** required for planet imaging will require coronagraphy to suppress PSF diffraction features. **Does it also require a simultaneous differential imager, or a low-resolution IFU?**

In many cases, **near-IR tip-tilt sensing** is required given the intrinsic redness of the science targets (e.g. brown dwarfs) or the high extinction of the science regions (e.g. star-forming regions). **Both on-axis and off-axis sensing will be needed**, depending on the optical/IR brightness of the primary stars. For off-axis science applications, sky coverage of $>30\%$ (as an areal average over the entire sky) is needed at the highest image quality over a corrected field of view of $< 5''$ in size.

Low-resolution (R \sim 100) near-IR (0.9-2.5 micron) spectroscopy **Question: how essential is 0.9 micron? Would 1 micron do?** is essential to follow-up planet discoveries, in order to determine their temperatures, surface gravities, and masses. The relevant spectral features have broad wavelength ranges, e.g. the broad-band SEDs of circumstellar dust needed to diagnose grain composition and sizes and the broad molecular absorption band of H₂O and CH₄ present in the atmospheres of ultracool brown dwarfs and extrasolar planets. **Does this low resolution spectroscopy have to be a spectrograph? Can it just use narrow-band filters?**

Thermal (L-band) imaging would be desirable to help measure the SEDs of the planets, but is not essential for this science.

2.2.4 Performance Requirements

2.2.4.1 Wavefront error

The key performance driver for this science case is contrast, not wavefront error. Initial simulations with an RMS wavefront error of 140 nm indicated that the required contrast could be achieved. Internal wavefront calibration errors of **TBD nm** will also be required of the AO system. **Note: need to repeat simulations for values of wavefront error larger than 140 nm (e.g. 170nm, 200 nm).**

2.2.4.2 Encircled energy

N/A

2.2.4.3 Generalized anisoplanatism

Required FOV is only a few (<5") arcseconds.

2.2.4.4 Photometric precision

Not a key requirement. Relative photometry of planetary companion to primary star of better than 0.05 mag, or absolute photometry of planetary companion to the same accuracy. **Need to explain further: the requirement for relative photometry of a very faint planet of 0.05 mag, with use of a coronagraph, could be quite difficult. Is this a requirement or not?**

2.2.4.5 Astrometric precision

Not a key requirement. Astrometric accuracy to ~1/10 of the PSF FWHM would suffice for proper motion confirmation that candidate planets are physically associated to their primaries.

2.2.4.6 Contrast

From a science standpoint, the required contrast can be set by the need to directly image Jupiter-mass planets around a large sample of (1) field low-mass stars and brown dwarfs at ages of <~200 Myr and (2) young stars in the nearest star-forming regions. A benchmark value of $\Delta(H)=13$ magnitudes at 1" separation is required.

2.2.4.7 Polarimetric precision

N/A

2.2.4.8 Backgrounds

Thermal L-band photometry is desirable, but not a key requirement.

2.2.4.9 Overall transmission

For some targets with low-mass primaries (brown dwarfs) and relatively old ages, high sensitivity will be a benefit at separations of $\geq 1''$. The baseline sensitivity numbers from the NGAO proposal of H=25 mag (5-sigma) in 20 minutes of on-source integration time are suitable for these purposes.

2.2.5 Other key design features

2.2.5.1 Required observing modes

On-axis and off-axis imaging and spectroscopy will be standard. Coronagraphic imaging will require some additional care to center the science target on the focal plane mask and to keep it there during the observations.

2.2.5.2 Observing efficiency

Good efficiency is required, i.e. 10 min or less overhead per target, since we want to be able to observe many (several dozen) targets per night.

2.2.6 Instrument requirements

Does this science case need a differential imager of some sort? If so, need to write down specs and think about capabilities.

2.2.6.1 Field of view

No more than $10''$.

2.2.6.2 Field of regard

All-sky average for off-axis observations should be $>30\%$.

2.2.6.3 IFU multiplicity

One object at a time only.

2.2.6.4 Wavelength coverage

0.9-2.5 microns (extension to L-band desirable, but not essential). Question: would 1 micron do? How important is 0.9 micron? Is a differential imager (simultaneous) needed?

2.2.6.5 Spectral resolution

R~100 at 0.9-2.5 microns. Question: would 1 micron do? How important is 0.9 micron?

2.2.7 References

To be DONE

2.3 Precision Astrometry: Measurements of General Relativity Effects in the Galactic Center

Authors: Andrea Ghez and Jessica Lu

Editor: Claire Max

2.3.1 Scientific background and goals

The proximity of our Galaxy's center presents a unique opportunity to study a massive black hole (BH) and its environs at much higher spatial resolution than can be brought to bear on any other galaxy. In the last decade, near-IR observations with astrometric precisions of < 1 mas and radial velocity precision of 20 km/s have enabled the measurement of orbital motions for several stars near the Galactic center (GC), revealing a central dark mass of $3.7 \times 10^6 M_{\text{sun}}$ (Ghez et al. 2003, Ghez et al. 2005; Schodel et al. 2002; Schodel et al. 2003). Radio VLBA observations have now resolved the central object to within several multiples of the event horizon, indicating that the central mass is confined to a radius smaller than 1 AU (Shen et al. 2005). These observations provide the most definitive evidence for the existence of massive BHs in the centers of galaxies. The orbital motions now also provide the most accurate measurement of the GC distance R_0 , constraining it to within a few percent (Eisenhauer et al. 2003).

2.3.2 General Relativistic Effects

Due to the crowded stellar environment at the GC and the strong line-of-sight optical absorption, tracking the stellar orbits requires the high angular resolution, near-IR imaging capabilities of adaptive optics on telescopes with large primary mirrors, such as Keck. Though the current orbital reconstructions are consistent with pure Keplerian motion, with improved astrometric and radial velocity precision deviations from pure Keplerian motion are expected. With Keck NGAO we will be able to detect the deviations from Keplerian motion due to a variety of effects. These will provide a unique laboratory for probing the dynamics of galactic nuclei, the properties of exotic dark matter, and the mass function of stellar-mass black holes. They will also provide the first tests of general relativity in the high mass, strong gravity, regime. Keck NGAO will measure these non-Keplerian motions to precisions that will not be greatly surpassed even in the era of extremely large (~ 30 m) telescopes.

Of the theories describing the four fundamental forces of nature, the theory that describes gravity, general relativity (GR), is the least tested. In particular, GR has not been tested in the strong field limit, on the mass scale of massive BHs. The highly eccentric 15 yr orbit of the star S0-2 brings it within 100 AU of the central BH, corresponding to ~ 1000 times the BH's Schwarzschild radius (i.e., its event

horizon). Studying the pericenter passage of S0-2 and the other high eccentricity stars therefore offers an opportunity to test GR in the strong gravity regime.

With Keck NGAO, the orbits can be monitored with sufficient precision to enable a measurement of post-Newtonian general relativistic effects associated with the BH. This includes the prograde precession of orbits. As Figure 1 illustrates, the General Relativistic prograde precession can be measured even for single orbits of known stars (e.g., S0-2, $K=14.1$ mag) if we have an astrometric precision of $\sim 100 \mu\text{s}$ coupled with a radial velocity precision of 10 km/s.

With Keck NGAO, the orbits can be monitored with sufficient precision to enable a measurement of post-Newtonian general relativistic effects associated with the BH. This includes the prograde precession of orbits. As Figure 1 illustrates **need to fix figure numbers**, the General Relativistic prograde precession can be measured even for single orbits of known stars (e.g., S0-2, $K=14.1$ mag) if we have an astrometric precision of $\sim 100 \mu\text{s}$ coupled with a radial velocity precision of 10 km/s.

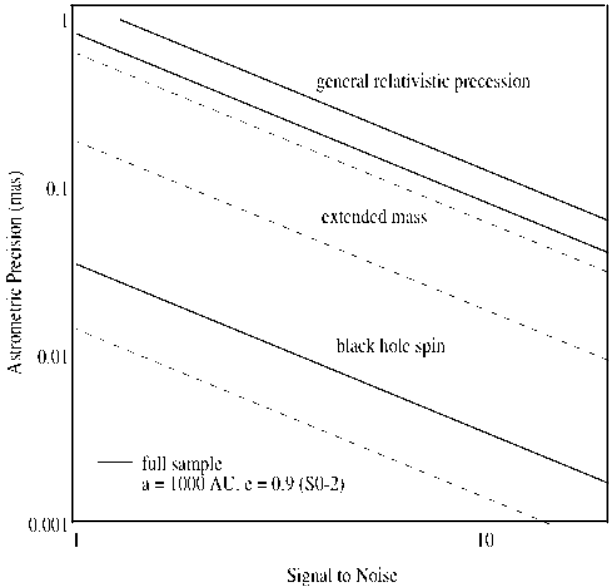


Figure 1. Required astrometric precision for detecting, from top to bottom, GR effects associated with relativistic prograde precession, extended mass within the stellar orbits, and frame-dragging effects due to BH spin (based on Weinberg et al. 2005). Estimates are based on measurements of stellar orbits and positions from Keck diffraction-limited images (thick, solid lines), and assume radial velocity measurement errors of 10 km/s. The stellar orbits include 16 stars within $0.5''$ of Sgr A* with orbital fits obtained from speckle imaging measurements and 142 stars within $1''$ of Sgr A* with stellar positions obtained with new, deep AO maps. For comparison, we also show estimates based on measurements from just the short-period star S0-2 (thin, dashed line). Results are for a 10-year baseline with 10 integrations per year. Low-order GR and extended matter effects are detectable at the $>7\sigma$ level if an astrometric precision of $\sim 100 \mu\text{s}$ can be achieved. Detection of BH spin requires either better precision or, at $\sim 100 \mu\text{s}$ precision, improved SNR obtained by observation of multiple as-yet-undiscovered high-eccentricity, short-period stars over multiple orbits.

Keck NGAO will bring several important improvements to measurements at the Galactic Center:

1) Current measurements are strongly confusion limited, because the Galactic Center is a very crowded field. Higher Strehl at K-band will improve contrast and therefore reduce the confusion, improving both photometric and astrometric accuracy because the previously undetected faint star population will cause less of a bias in the positions and magnitudes of brighter stars.

2) Higher Strehl at K-band will allow the detection of new stars, some of which may pass close enough to the black hole to contribute to the obtainable accuracy and precision of General Relativistic effects. (See figure caption.)

3) NGAO's use of multiple laser guide stars and multiple IR tip-tilt stars will decrease the field dependence of the PSF, thereby increasing both photometric and astrometric accuracy. This effect needs to be quantified.

4) The accuracy of current radial-velocity measurements is limited by signal to noise. NGAO's higher Strehl and lower sky background will materially improve the radial-velocity contribution to orbit determinations.

2.3.3 R_0 and the dark matter halo

Since the orbital periods are proportional to $R_0^{3/2}M_{\text{bh}}^{-1/2}$ and the radial velocities are proportional to $R_0^{-1/2}M_{\text{bh}}^{1/2}$, where R_0 is the heliocentric distance to the BH and M_{bh} its mass, the two parameters are not degenerate and can be determined independently (Salim & Gould 1999). As shown in Figure 1, by complimenting high precision astrometric measurements with high precision radial velocity measurements with accuracies of $\sim 10 \text{ km s}^{-1}$, we can measure R_0 to an accuracy of only a few parsecs (i.e., $\sim 0.1\%$ accuracy) with Keck NGAO. Today's radial velocity precision for the observations in hand is about 20 km/s. This could be improved upon with higher signal to noise observations, either from longer integration times or lower backgrounds.

Since R_0 sets the scale within which is contained the observed mass of the Galaxy, measuring it to high precision enables one to determine to equally high precision the size and shape of the Milky Way's several kpc-scale dark matter halo (Olling & Merrifield 2000). The halo shape tells us about the nature of dark matter (e.g., the extent to which it self-interacts) and the process of galaxy formation (how the dark matter halo relaxes following mergers). Currently the shape is very poorly constrained.

2.3.4 Proposed observations and targets

Target: Central 10 arc sec of the Galactic Center, centered on SgrA*. Note that this is a low-elevation target from Keck (RA 17 45 40 DEC -29 00 28).

Observing wavelengths: K band (2.2 microns)

Observing mode: Imaging for astrometry purposes, and spectroscopy for radial velocities

2.3.5 Observing plan for Astrometric Imaging:

Based upon a description of how things are done today using 1st-generation Keck AO:

a) Guide Star Acquisition:

Current visible-wavelength guide star is **USNO-A2.0 0600-28577051** (R=14.0, Separation = 19.3'')

There are a great many possible IR tip-tilt stars, as shown in Appendix A. The addition of multiple IR-corrected tip-tilt stars is anticipated to improve astrometric accuracy considerably, although more work is needed in order to understand the limitations of today's observations.

- b) 1-minute K' exposures, continuing for 3.5 hours elapsed time
- c) Dither pattern is random over a 0.7'' box (small box used to minimize distortion)
- d) Construct 40 arcsec mosaics to tie to radio astrometric reference frame (radio masers)
- e) After the Galactic Center has set, move to a dark patch of sky at a similar airmass to obtain sky exposures.

Standard stars: none (astrometry)

Data Analysis:

1. Image reduction is standard, including distortion correction using the NIRC2 pre-ship review distortion solution. Improved distortion solution is needed and appears to be possible with data in hand.
2. Individual exposures are shifted (translations only) and added together for an entire night to produce a final map. Information from >1000 stars (what is this number) is included in the solution.
3. Individual exposures are also divided into 3 subsets of equal quality to produce 3 images used for determining the astrometric and photometric RMS errors.
4. Source extraction is performed using StarFinder (Diolaiti et al, SPIE paper) which iteratively estimates the PSF from several bright stars in the image

and then extracts all source positions and photometry.

5. Star lists from different epochs are aligned by matching all the stars (what is this number) and minimizing the quad-sum of their offsets allowing for a 2nd order transformation between epochs.

2.3.6 Observing plan for Radial Velocity Measurements (IFU spectroscopy):

K-band IFU spectroscopy, one field

20 or 35 mas plate scale, R~4000

FOV at least 1.0'' x 1.0''

Exposure times are currently 15 minutes.

Sky frames of the same duration are obtained in the same mode after the Galactic Center sets in order to remove OH lines.

Obtain standards of A and G spectral type to remove telluric lines.

Data analysis performed with a provided pipeline to do wavelength calibration.

2.3.7 Current issues and limitations that could be further explored with existing data sets

1) Improved geometric distortion map for narrow camera on NIRC2. At present we know that the map from pre-ship review is incorrect at the half-pixel level.

2) Effect of differential tip-tilt error across 10 arc sec field. Present data shows the expected decrease in astrometric errors as the stars get brighter ($K=20 \rightarrow 15$), due to photon noise improvement. However for stars brighter than $K=15$, the astrometric error hits a plateau and does not improve further as the stars get brighter. This is illustrated in Figure 2. (Need to fix figure numbers) The Galactic Center Group at UCLA has three hypotheses for the existence of this floor: differential tip-tilt anisoplanatism across the field, differential high-order anisoplanatism across the field, and/or lack of a good enough distortion solution for the narrow camera. At present the Galactic Center Group thinks the most likely cause is differential tip-tilt anisoplanatism; they plan to test this hypothesis by further analysis of existing data.

3) In principle chromatic and/or achromatic atmospheric refraction could be adversely affecting current accuracy. These effects will also be analyzed further.

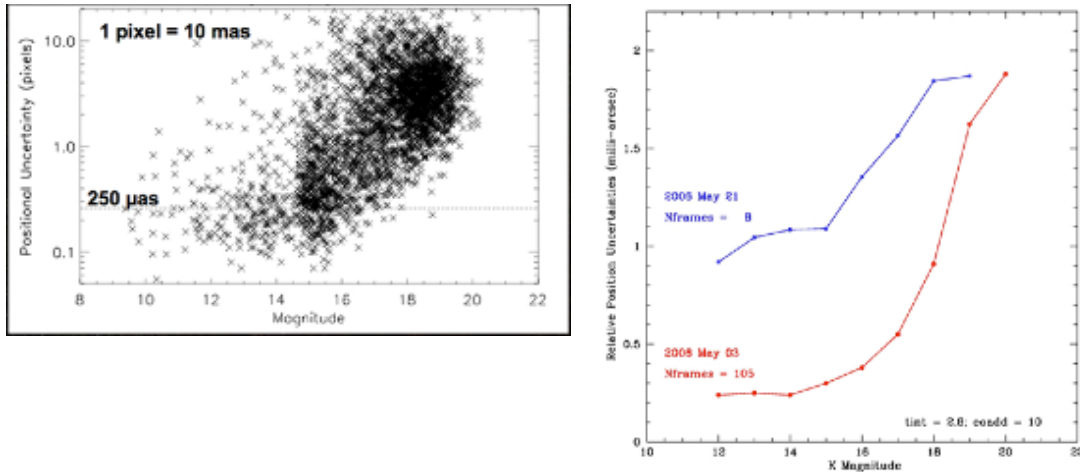


Figure 2. Left panel: positional uncertainty vs. stellar magnitude for stars near Galactic Center. Pixel scale is 0.01 arc sec/px. Right panel: average values of positional uncertainties for two different data sets. The positional uncertainty of the “floor” changes from about 1 mas to 0.25 mas between the two data sets shown.

2.3.8 AO requirements

Astrometry:

| | |
|------------------------|---|
| Astrometric precision | 100 micro arc sec or better |
| Wavefront error | 170 nm or better (need to study sensitivity to WFE) |
| Tip-tilt correction | IR tip-tilt needed; due to very strong reddening in Galactic Center, available J-band stars will be fainter than at H or K band. The total astrometric precision should be better than 0.1 mas. Therefore the required contribution from differential tip-tilt must be smaller than this. Further investigation into the astrometric error budget is required to determine the exact requirement. |
| Photometric precision | na |
| Polarimetric precision | na |
| Backgrounds | na (confusion dominated) |

2.3.9 General comments on astrometric accuracy in an AO system with multiple deformable mirrors

One of the point design concepts for Keck NGAO specifies a large-stroke deformable mirror within the main optical relay, plus a high-order MEMS deformable mirror either located on-axis or in multiple deployable IFU arms. Any AO system with multiple DMs must consider the impacts on astrometric accuracy. The following is a quote from the TMT Science-Driven Requirements Document

that seems relevant to Keck NGAO design as well (this should be regarded as a place-holder for future NGAO-specific analysis of the same topic):

“An astrometric MCAO system must constrain Zernike modes 4-6 using either a single natural guide star (NGS) which is bright enough to sense defocus and astigmatism or provide two additional tip-tilt stars, making their total number 3. The differential tilts between the three tip-tilt stars constrain these modes. This requirement occurs because the tip and tilt of laser guide stars (LGS) are undetermined. As a consequence, the information brought by them is insufficient for a full solution of the tomographic problem. In addition to tip and tilt, differential astigmatism and defocus between the two DMs is unconstrained. These three unconstrained modes do not influence on-axis image quality, but produce differential tilt between the different parts of the field of view.

If multiple tip-tilt sensors are used, the MCAO system must provide for a facility to align them. If the tip-tilt sensors for the three NGSs are misplaced, the MCAO system will compensate these errors in the closed loop, hence the field will be distorted. For example, the plate scale will change if the upper DM has a static defocus. Calibration procedures must be applied to ensure that these errors do not compromise the astrometric performance of an MCAO system (e.g., flattening of the upper DM before closing the loop).

The limitations on astrometric accuracy imposed by the atmosphere are discussed in detail in TMT technical report #XX (Graham 2003)”.

2.3.10 Radial Velocity:

IFU with 20 or 35 mas slitlets/spaxels

The required radial velocity accuracy is 10 km/s which is a factor of 2 improvement over current observations with OSIRIS-LGSAO. Current accuracy is limited by:

- 1) Signal-to-noise:
 - this will be improved by higher Strehl ratios.
- 2) Differential atmospheric refraction (chromatic):
 - should be compensated for by an infrared atmospheric dispersion corrector.
- 3) PSF estimation:
 - Should investigate how to improve PSF estimation for fields without good PSF stars.
- 4) Local background subtraction (diffuse Br-gamma gas over the entire field):
 - Higher Strehls will yield sky estimates that are less contaminated by the halos of bright stars.
- 5) spectral resolution (many lines are blends):
 - Br-gamma (2.166 microns) and He (2.112 microns) lines are blends at $R \sim 4000$. Higher spectral resolution would resolve the individual lines. Further investigation of the ideal spectral resolution is needed.

2.3.11 Instrument requirements

Essential: High contrast near-IR imager with excellent astrometric performance.

Essential: Infrared integral field spectrometer, $R \geq 3000$

Desirable but not absolutely essential: High resolution ($R \sim 15000$) IFU spectroscopy. With this spectral resolution, radial velocity accuracies are improved to ~ 1 km/s and the radial velocity measurements may themselves constrain General Relativistic effects.

Imager:

Field of view: at least $10'' \times 10''$

Field of regard: IR tip-tilt stars available $1-20''$ from imaging field center.
Tip-tilt pickoff is required to be able to deal with multiple tip-tilt stars separated by only a few arcseconds.

IFU multiplicity: one is sufficient

Wavelength coverage: K-band (2.2 microns)

IFU Spectrometer:

Field of view: at least $1'' \times 1''$

Field of regard: as needed to meet tip-tilt correction requirements

IFU multiplicity: one is sufficient

Wavelength coverage: K-band

Spectral resolution: $R > 3000$ (in addition, optional $R \sim 15,000$)

Type and depth of required data pipeline: IFU pipeline for wavelength/flux calibration

2.3.12 References

Broderick, A. E., & Loeb, A. 2005, MNRAS, 363, 353

Diolaiti, E., 0. Bendinelli, D. Bonaccini et al. 2000, A&AS 147, 335

Eisenhauer, F., Schodel, R., Genzel, R., Ott, T., Tecza, M., Abuter, R., Eckart, A., & Alexander, T. 2003, ApJL, 597, L121

Genzel, R., Schodel, R., Ott, T., Eckart, A., Alexander, T., Lacombe, F., Rouan, D., & Aschenbach, B. 2003, Nature, 425, 934

Ghez, A. M., Salim, S., Hornstein, S. D., Tanner, A., Lu, J. R., Morris, M., Becklin, E. E., & Duchene, G. 2005, ApJ, 620, 744

Ghez, A. M., et al. 2004, ApJL, 601, L159

Ghez, A. M., et al. 2003, ApJL, 586, L127

Gondolo, P., & Silk, J. 1999, Physical Review Letters, 83, 1719

Miralda-Escude, J., & Gould, A. 2000, ApJ, 545, 847

Morris, M. 1993, ApJ, 408, 496
Olling, R. P., & Merrifield, M. R. 2000, MNRAS, 311, 361
Peebles, P. J. E. 1972, ApJ, 178, 371
Salim, S., & Gould, A. 1999, ApJ, 523, 633
Schodel, R., Ott, T., Genzel, R., Eckart, A., Mouawad, N., & Alexander, T. 2003, ApJ, 596, 1015
Schodel, R., et al. 2002, Nature, 419, 694
Shen, Z.-Q., Lo, K. Y., Liang, M.-C., Ho, P. T. P., & Zhao, J.-H. 2005, Nature, 438, 62
Weinberg, N. N., Milosavljevic, M., & Ghez, A. M. 2005, ApJ, 622, 878

2.4 Resolved Stellar Populations in Nearby Galaxies

The text below is quoted from the TMT SRD, with appropriate modifications. Work on Keck NGAO-specific science and AO issues is in progress, and will replace the text below in a subsequent release of this document.

The “in situ” study of the process of galaxy formation in which galaxies are observed at large z and lookback time has begun with Keck’s first-generation AO system and will be considerably enhanced by NGAO. A powerful alternative approach to understanding the processes of galaxy formation and evolution is to use the $z = 0$ stellar “fossil record”. The basic understanding of the star formation, chemical evolution, and accretion history of the Galaxy was developed based on color-magnitude diagram studies, abundances of elements in stars from different Galactic populations, and the relations between stellar kinematics, ages and metallicities. In the past decade, using the Hubble Space Telescope and 4m – 10m ground-based telescopes, studies based on resolved stellar populations have been extended to the Galaxy’s dwarf galaxy complement. This work has revealed an unexpectedly wide variety of star formation and chemical enrichment histories for the handful of galaxies for which such studies have been possible.

This is a field that benefits directly from improved Strehl and improved knowledge of the PSF. Resolved-stellar-content studies can be extended by NGAO throughout the Local Group and to groups within 10-20Mpc, including perhaps populations in the outer reaches of galaxies in the Virgo cluster.

Key questions to be addressed are:

- What is the star formation history for galaxies through the Hubble Sequence?
- What is the range of star formation history at a given Hubble Type?
- What are the key factors that govern dwarf galaxy star formation episodes?
- What is the assembly/star formation history for a giant elliptical galaxy based on resolved-star analysis?
- Did star formation commence at the same time for all galaxies in the local universe?
- Are today’s integrated-light abundance and age studies of distant galaxies accurate?
- Are the star formation histories of local galaxies compatible with observations of galaxies at large lookback times and can a mapping be established between galaxies at different epochs of the Universe?

2.5 Galaxy Assembly and Star Formation History

Authors: D. Law, C. Steidel, J. Larkin

Editor: Claire Max

2.5.1 Introduction

Within the last decade the near infrared has become crucial for understanding the early universe and the evolution of galaxies. At redshifts above 1, galaxies have shrunk to angular sizes of approximately 1 arcsec making seeing based observations almost useless at uncovering morphologies and internal kinematics. At the epoch of greatest star formation and AGN activity around a redshift of 2.5, the traditional optical lines of H α , OIII and OII are nicely shifted into the K, H and J bands respectively. The combination of the Keck LGS AO system with OSIRIS spatially resolved infrared spectroscopy is just now starting to dissect some of the brightest galaxies at this epoch. But with the factor of ~ 10 in sensitivity gain possible with Keck NGAO, a wealth of science topics can be addressed. These include the relationship between AGN and their host galaxies: radio galaxies and quasars have very strong emission lines and complex kinematics. In more “normal” galaxies, the redshift range from 1.5 to 2.5 is the key era for the birth of their first stars and the formation of the major architectural components, namely the bulge and disk. Measuring the morphology of star formation, the kinematics of proto-disks, the internal velocity dispersions and metallicity gradients (from things like the NII/H α ratio) will allow us to witness the birth of galaxies like the Milky Way.

Table 1 gives a sample of which lines are available as a function of redshift.

| Redshift | J band | H band | K band |
|------------|------------|------------|------------|
| ~ 1.2 | H α | | |
| ~ 1.5 | OIII | H α | |
| ~ 2.5 | OII | OIII | H α |
| ~ 3.2 | | OII | OIII |
| ~ 4.1 | | | OII |

Because JWST is optimized for faint-object IR spectroscopy and imaging, for this science case we will have to seek specific “sweet spots” in which Keck NGAO can make a significant contribution in the age of JWST.

Below we address the science requirements flowing from one of these redshift ranges: $2 \leq z \leq 3$.

2.5.2 Scientific background and context: galaxies at $2 \leq z \leq 3$

At high redshifts $z \sim 2-3$ galaxies are thought to have accumulated the majority of their stellar mass (Dickinson et al. 2003), the rate of major galaxies mergers appears to peak (Conselice et al. 2003), and instantaneous star formation rates and stellar

masses range over two decades in value (Erb et al. 2006). Given the major activity at these redshifts transforming irregular galaxies into the familiar Hubble sequence of the local universe, it is of strong interest to study these galaxies in an attempt to understand the overall process of galaxy formation and the buildup of structure in the universe.

The global properties of these galaxies have recently received considerable attention, and the star formation rate, stellar mass, gaseous outflow properties, etc. have been studied in detail (e.g. Steidel et al. 2004, Papovich et al. 2006, Reddy et al. 2006 and references therein). Beyond these global properties however, little is known about their internal kinematics or small-scale structure, particularly with regard to their mode of dynamical support or distribution of star formation. Previous observations with slit-type spectrographs (e.g. Erb et al. 2004, Weiner et al. 2006) and seeing-limited integral field spectrographs (Flores et al. 2006) suggest that kinematics are frequently inconsistent with simple equilibrium disk models. However these studies are too severely constrained by slit misalignment, spatial resolution, and the size of the atmospheric seeing halo relative to the size of the typical sources (less than one arcsecond) to obtain conclusive evidence. It is therefore unknown whether the majority of star formation during this epoch is due to rapid nuclear starbursts driven by major merging of gas-rich protogalactic fragments, circumnuclear starbursts caused by bar-mode or other gravitational instabilities, or piecemeal consumption of gas reservoirs by overdense star forming regions in stable rotationally-supported structures.

Here we investigate the general capabilities of Keck NGAO for the study of these high-redshift galaxies, via simulations of the integral field spectrographs used to dissect these galaxies and to study their kinematics and chemical composition.

2.5.3 Scientific goals

The study of high-redshift galaxies is a powerful driver for multiplexed observations, for example via deployable integral field unit (IFU) spectrographs. Given the areal densities of 1 to 10 targets per square arcminute on the sky (depending on the target selection criteria: Table 1 **fix Table numbers**), multiplexing multi-conjugate or multi-object adaptive optics (MCAO/MOAO) systems would be capable of simultaneously observing ~ 10 targets within a 5 square arcminute field, permitting the compilation of a large representative sample with a minimum of observing time. In order to take best advantage of the high areal densities of targets, it is desirable to be able to deploy of order 6-12 IFUs over a given 5 square arcminute field of view.

Table 1 Space Densities of Various Categories of Extragalactic Targets.

| Type of Object | Approx density per square arc minute | Reference |
|--|---|--|
| SCUBA sub-mm galaxies to 8 mJy | 0.1 | Scott et al. 2002 |
| Old and red galaxies with $0.85 < z < 2.5$ and $R < 24.5$ | 2 | Yamada et al. 2005; van Dokkum et al. 2006 |
| Field galaxies w/ emission lines in JHK windows $0.8 < z < 2.6$ & $R < 25$ | > 25 | Steidel et al 2004; Coil et al 2004 |
| Center of distant rich cluster of galaxies at $z > 0.8$ | > 20 | van Dokkum et al 2000 |
| All galaxies $K < 23$ | > 40 | Minowa et al 2005 |

Such observations would permit the study of the chemical composition and distribution of star formation within the target galaxies (e.g. through mapping the measured [N II]/H α ratios), in addition to mapping the velocity fields of the galaxies. Velocity data will enable the detection of AGN through chemical signatures and broadening of nuclear emission lines, differentiate chaotic major mergers from starbursting galaxies in dynamical equilibrium, determine the location of major star forming regions within any such rotationally supported systems, and permit the distinction between chaotic and regular velocity fields to help ascertain whether observed star formation is commonly a consequence of major tidal interaction as predicted in current theories of galaxy formation.

With current-generation instruments, it is extremely challenging to observe a representative sample of sources due to the uncertainties inherent in long-slit spectroscopy (i.e. slit misalignment with kinematic axes), seeing-limited integral field spectroscopy (i.e. loss of information on scales smaller than the seeing disk), or a single-object IFU with current-generation adaptive optics (for which integration times are prohibitive for obtaining a large sample). As such, a high-Strehl NGAO system with multi-object IFU capability would represent a major advance towards obtaining reliable kinematic and chemical data for a large sample of high redshift galaxies which could be productively integrated with the known global galaxy properties to further our understanding of galaxy formation in the early universe.

2.5.4 Proposed observations and targets

At redshifts $z = 0.5-3$, major rest-frame optical emission lines such as H α , [N II], and [O III] fall in the observed frame near-IR, and in order to study the evolution of galaxies across this range of cosmic times it is important to have wavelength coverage extending from 1 to 2.5 microns. H α line emission from the well-studied redshift $z \sim 2-3$ galaxy sample falls in the K band, emphasizing the importance of

optimizing observations at these wavelengths by reducing backgrounds and increasing throughput as much as possible.

Typical observing strategy would entail simultaneous observation of approximately 10 high-redshift galaxies in a given field using a dithered set of exposures designed to move each object around on the detectors permitting maximum on-source integration time whilst simultaneously measuring accurate background statistics for sky subtraction. Based on the numerical simulations of Law et al. (2006) and the observed performance of the OSIRIS spectrograph, we anticipate that typical observations (assuming a K-band Strehl of roughly 60-70% from the NGAO system) would last approximately 1-2 hours per set of targets (for bright star-forming galaxies at redshift $z \sim 2$) permitting a sample of approximately 50 targets in a given night of dedicating observing.

2.5.5 AO and instrument requirements

Using the Gemini model of the Mauna Kea near-IR sky background coupled with a mathematical model of the thermal contributions from warm optical surfaces in the light path, Law et al. (2006) have demonstrated that the current K-band performance of AO-fed instruments is limited primarily by thermal emission from the warm AO system (which constitutes the majority of the total interline K band background). It is therefore a priority to reduce this emission to a small fraction of the intrinsic background from the night sky and thermal radiation from the telescope itself. Using a combination of high-throughput optical components and AO system cooling, we require that thermal radiation from the AO system contribute less than 10-20% to the total K-band background. In Figure 1, we plot the cooling required (according to the Law et al. 2006 models) as a function of the throughput to achieve this goal.

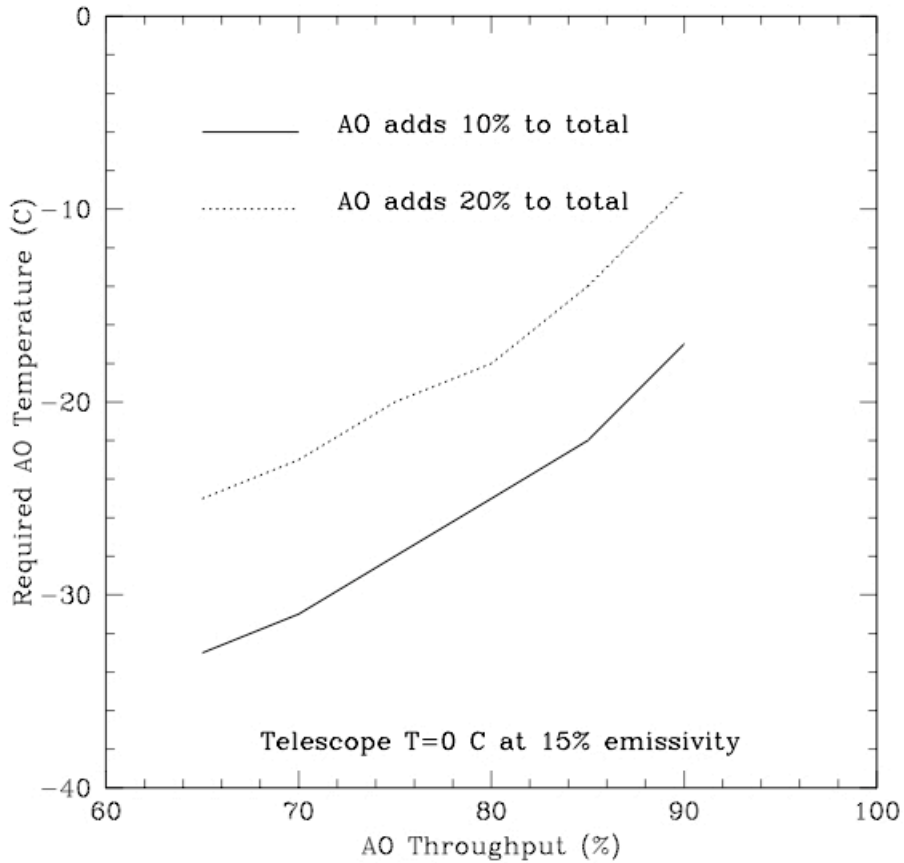


Figure 1: Required AO system temperature as a function of AO throughput to minimize impact of thermal radiation on the net K-band background.

Given the typical size of the target galaxies (less than or of order an arcsecond), the field of view of each IFU should be suitably large to permit accurate sky subtraction (via on-IFU dithering) while sampling the target on the smallest scales permitted by detector noise characteristics. That is, each IFU should have a field of view measuring at least 3×1 arcseconds in order to avoid costly dedicated sky exposures, and should be sampled on scales of order the diffraction limit (~ 50 mas) to permit more accurate characterization of the structure on small scales without introducing excessive instrumental contribution to the total noise budget. Spectral resolution should be greater than $R \sim 3000$ in order to effectively resolve out OH sky features and distinguish $H\alpha$ from [N II] emission.

2.5.5.1 AO Requirements

Specifying AO requirements such as spatial resolution and encircled energy is not straightforward for the high- z galaxy science case. This is because the width of the core of the PSF will be limited by the availability of adequately bright tip-tilt stars. One can obtain excellent spatial resolution and encircled energy over that small

fraction of the sky where excellent tip-tilt stars are available, or more modest spatial resolution and encircled energy over a larger fraction of the sky. AO requirements that deal with resolution alone are less useful than those that can be phrased in terms of “spatial resolution of xx achieved over a sky coverage fraction larger than yy”. As we have not yet worked through this type of specification, we present the resolution and encircled energy requirements in terms of the desired IFU spaxel size, 50 mas.

AO Requirements:

Spaxel size (IFU spectroscopy)
Field of view of one IFU unit

Backgrounds
Field of regard
Is a contiguous field required?
Encircled energy (80%? 50%?)
Sky coverage fraction

(Photometric accuracy)
(Astrometric accuracy)
(Polarimetry)
(Contrast sensitivity)

Near-IR

50 mas
3 x 1 arc sec or greater
(object size ~ 1”, but need 3” in at least one dimension to get good sky meas’t)
< 10-20% above telescope plus sky
As large as needed to get tip-tilt stars
no
50 mas with optimal tip-tilt stars
at least 30% with encircled energy
radius < 75 mas

2.5.5.2 Instrument Requirements:

| | |
|------------------------------|--|
| Field of view (spectroscopy) | 3 x 1 arc sec or greater (e.g. 3 x 1 arcsec for 5% bandpass, 3 x 3 arsec for 20% bandpass) |
| Field of regard | As large as needed for good tip-tilt |
| IFU or imager multiplicity | 6-12 |
| Wavelength coverage | JHK |
| Spectral resolution | 3000 - 4000 |
| Data reduction pipeline | Required |
| Other considerations | Atmospheric dispersion: may be able to avoid a dispersion corrector through appropriate data reduction pipeline software |

2.5.6 References

Conselice et al. 2003, AJ, 126, 1183
Dickinson et al. 2003, ApJ, 587, 25
Erb et al. 2004, ApJ, 612, 122
Flores et al. 2006, astro-ph/0603563
Law et al. 2006, AJ, 131, 70

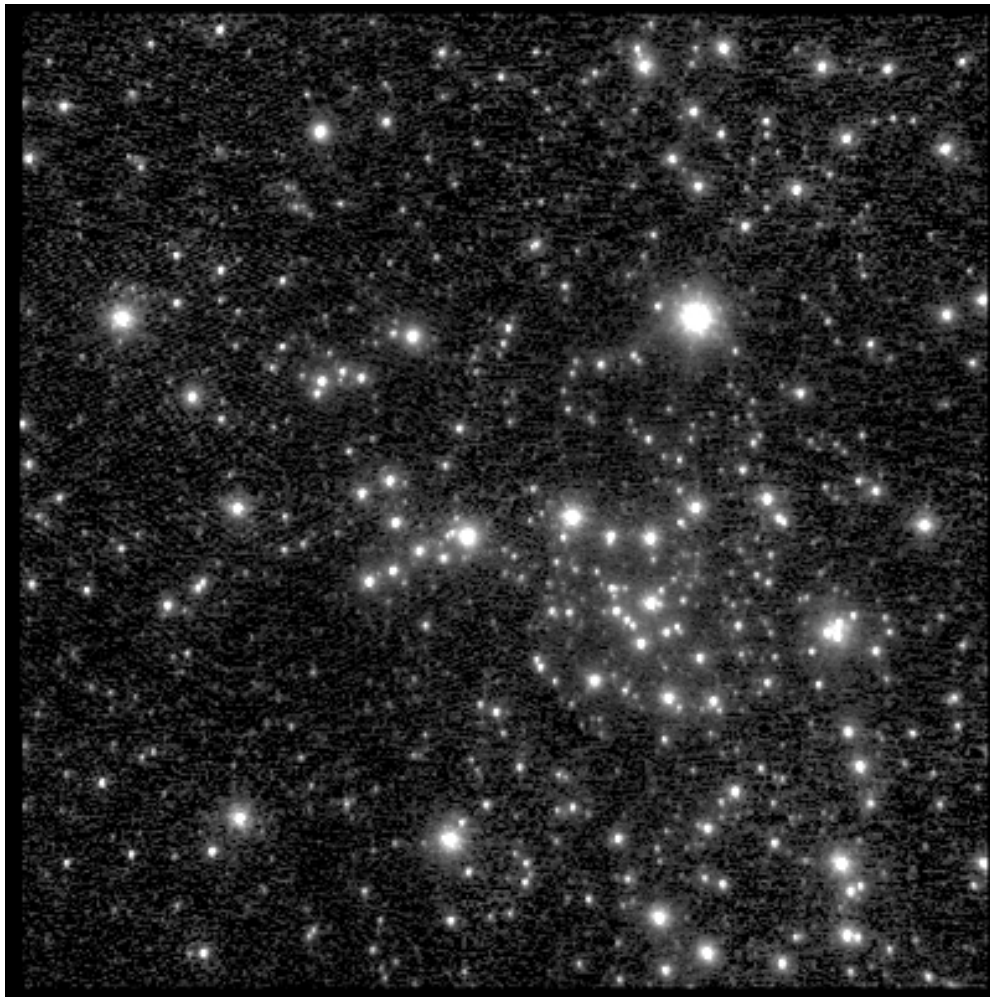
Papovich et al. 2006, ApJ, 640, 92

Reddy et al. 2006, ApJ, 644, 792

Weiner et al. 2006, astro-ph/0609090

3 Appendix A. Table of potential infrared tip-tilt stars close to the Galactic Center

Figure A1. Mosaic of Galactic Center at K band, from J. Lu and A. Ghez. The FITS file of this observation, which includes the WCS coordinate system, is available for use in correlating the image with the tables that follow.



Following pages: Tables from Blum et al. 1996, ApJ 470, 864

TABLE 1
GALACTIC CENTER OBSERVED PHOTOMETRY

| ID | Name | $\Delta\alpha$ (arcsec) ^a | $\Delta\delta$ (arcsec) ^a | K | $J-K$ | $H-K$ | $K-L$ | Notes |
|---------|----------|--------------------------------------|--------------------------------------|--------------|-------------|-------------|-------------|---------|
| 1..... | | -40.07 | -8.01 | 10.40 ± 0.08 | ... | ... | ... | |
| 2..... | | -38.31 | -22.60 | 10.27 ± 0.05 | ... | ... | ... | |
| 3..... | | -37.55 | 6.96 | 10.10 ± 0.05 | ... | ... | ... | |
| 4..... | | -34.38 | -18.66 | 10.36 ± 0.04 | 6.85 ± 0.97 | 2.74 ± 0.06 | ... | |
| 5..... | | -29.36 | -23.17 | 10.26 ± 0.03 | 6.61 ± 0.06 | 2.62 ± 0.05 | ... | |
| 6..... | | -28.49 | -40.40 | 9.67 ± 0.03 | ... | ... | ... | |
| 7..... | | 26.91 | 18.90 | 9.80 ± 0.03 | 7.15 ± 0.06 | 2.76 ± 0.05 | ... | |
| 8..... | | 24.04 | 18.35 | 10.24 ± 0.06 | 6.65 ± 0.07 | 2.51 ± 0.07 | ... | |
| 9..... | | -23.04 | 16.43 | 9.92 ± 0.04 | 6.29 ± 0.05 | 2.42 ± 0.05 | ... | |
| 10..... | | -22.97 | 11.96 | 10.44 ± 0.04 | 7.11 ± 0.09 | 2.99 ± 0.05 | ... | |
| 11..... | | -22.40 | 41.86 | 9.22 ± 0.14 | ... | ... | ... | |
| 12..... | | -21.48 | 42.24 | 10.32 ± 0.08 | 5.34 ± 0.10 | 1.94 ± 0.11 | ... | |
| 13..... | | -20.12 | -32.15 | 10.06 ± 0.03 | 7.42 ± 0.07 | 3.33 ± 0.05 | ... | H92 |
| 14..... | | -19.30 | 25.37 | 10.48 ± 0.03 | 6.75 ± 0.05 | 2.68 ± 0.05 | ... | |
| 15..... | | -17.16 | 28.26 | 10.45 ± 0.03 | 6.27 ± 0.05 | 2.43 ± 0.05 | ... | H92 |
| 16..... | | -16.97 | 10.34 | 9.59 ± 0.03 | 4.78 ± 0.04 | 1.70 ± 0.04 | ... | H92 |
| 17..... | | -16.09 | 18.45 | 9.74 ± 0.03 | 6.07 ± 0.04 | 2.48 ± 0.05 | ... | |
| 18..... | | -13.72 | 15.34 | 10.18 ± 0.04 | ... | 3.16 ± 0.05 | ... | |
| 19..... | | -13.27 | -16.88 | 10.14 ± 0.03 | 7.57 ± 0.15 | 3.01 ± 0.05 | ... | H92 |
| 20..... | | -10.90 | -32.26 | 10.49 ± 0.04 | ... | 2.52 ± 0.05 | ... | |
| 21..... | | -9.76 | -25.81 | 10.24 ± 0.03 | 6.07 ± 0.05 | 2.24 ± 0.05 | ... | |
| 22..... | BSD WC9 | -9.69 | -11.54 | 10.74 ± 0.05 | ... | 2.08 ± 0.07 | ... | WC9 |
| 22..... | BSD WC9 | -9.69 | -11.54 | 10.72 ± 0.05 | ... | ... | ... | b |
| 23..... | | -9.59 | 6.47 | 9.75 ± 0.03 | 6.14 ± 0.04 | 2.31 ± 0.05 | ... | |
| 24..... | | 9.36 | -17.17 | 10.18 ± 0.04 | 5.53 ± 0.05 | 2.05 ± 0.06 | ... | |
| 25..... | AF NWB | 9.11 | -8.97 | 11.67 ± 0.14 | ... | ... | ... | b |
| 25..... | AF NWB | 9.11 | -8.97 | 11.60 ± 0.09 | 5.26 ± 0.10 | 2.37 ± 0.12 | ... | |
| 26..... | BSD WC9B | 9.08 | -11.90 | 12.07 ± 0.13 | ... | ... | ... | b |
| 26..... | BSD WC9B | 9.08 | -11.90 | 12.04 ± 0.14 | ... | 1.84 ± 0.18 | ... | |
| 27..... | | -9.05 | 34.75 | 9.02 ± 0.03 | ... | 2.66 ± 0.05 | ... | |
| 28..... | IRS 11 | -8.44 | 8.03 | 9.17 ± 0.07 | 5.95 ± 0.07 | 1.99 ± 0.08 | ... | Cool |
| 29..... | AF NW | -8.24 | -9.28 | 11.93 ± 0.17 | ... | ... | ... | h |
| 29..... | AF NW | -8.24 | -9.28 | 11.85 ± 0.11 | 5.15 ± 0.13 | 2.29 ± 0.15 | ... | He I |
| 30..... | IRS 6WB | -8.17 | -4.01 | 11.51 ± 0.42 | ... | ... | ... | h |
| 31..... | IRS 6W | -8.12 | -4.40 | 10.26 ± 0.14 | ... | ... | ... | h |
| 31..... | IRS 6W | -8.12 | -4.40 | 10.22 ± 0.05 | 5.78 ± 0.06 | 2.40 ± 0.07 | ... | |
| 32..... | AF B | -7.79 | -13.58 | 11.24 ± 0.07 | 5.25 ± 0.09 | 1.95 ± 0.09 | ... | |
| 33..... | AF | -7.28 | -12.89 | 10.74 ± 0.09 | ... | ... | ... | h |
| 33..... | AF | -7.28 | -12.89 | 10.70 ± 0.05 | 5.12 ± 0.06 | 2.06 ± 0.06 | ... | He I |
| 34..... | | -7.00 | -27.69 | 10.19 ± 0.06 | ... | 2.36 ± 0.07 | ... | b |
| 35..... | IRS 30 | -6.56 | 0.21 | 10.68 ± 0.08 | ... | ... | ... | |
| 35..... | IRS 30 | -6.56 | 0.21 | 10.49 ± 0.05 | 7.11 ± 0.16 | 2.49 ± 0.11 | 1.08 ± 0.23 | h |
| 36..... | | -6.47 | -22.39 | 10.37 ± 0.03 | 5.19 ± 0.04 | 1.85 ± 0.05 | ... | |
| 37..... | IRS 30B | -5.87 | -0.14 | 11.15 ± 0.16 | ... | ... | ... | |
| 38..... | IRS 6E | -5.53 | -5.08 | 10.06 ± 0.06 | ... | 4.26 ± 0.17 | ... | WC9 |
| 38..... | IRS 6E | -5.53 | -5.08 | 9.80 ± 0.06 | ... | ... | 2.96 ± 0.08 | b |
| 39..... | | -5.03 | -28.27 | 10.37 ± 0.04 | 6.20 ± 0.05 | 2.37 ± 0.05 | ... | |
| 40..... | | -4.89 | 33.81 | 10.09 ± 0.05 | ... | ... | ... | |
| 41..... | | -4.50 | 30.34 | 10.14 ± 0.09 | ... | 2.39 ± 0.10 | ... | |
| 42..... | IRS 13W | -4.45 | 7.80 | 10.96 ± 0.12 | ... | ... | ... | Cool |
| 42..... | IRS 13W | -4.45 | 7.80 | 10.61 ± 0.11 | ... | ... | 2.87 ± 0.20 | b |
| 43..... | | -4.29 | 21.77 | 10.07 ± 0.03 | 6.13 ± 0.05 | 2.29 ± 0.05 | ... | |
| 44..... | IRS 12NB | -4.16 | -13.61 | 10.10 ± 0.10 | 5.69 ± 0.11 | 2.43 ± 0.12 | ... | |
| 45..... | IRS 2 | -4.15 | -10.47 | 10.57 ± 0.06 | ... | 3.65 ± 0.13 | ... | Cool |
| 45..... | IRS 2 | -4.15 | -10.47 | 10.34 ± 0.09 | ... | ... | 2.29 ± 0.14 | b |
| 46..... | IRS 34 | -4.13 | -4.09 | 10.75 ± 0.07 | ... | ... | ... | He I |
| 46..... | IRS 34 | -4.13 | -4.09 | 10.48 ± 0.08 | ... | 2.83 ± 0.16 | 1.87 ± 0.19 | h |
| 47..... | IRS 12S | -4.10 | -14.63 | 9.95 ± 0.05 | 5.85 ± 0.06 | 2.18 ± 0.06 | ... | Cool |
| 48..... | IRS 22 | -3.90 | -31.98 | 8.03 ± 0.03 | 5.13 ± 0.04 | 1.77 ± 0.05 | ... | *, Cool |
| 49..... | IRS 2L | -3.87 | -9.64 | 11.68 ± 0.20 | ... | ... | 4.37 ± 0.21 | d |
| 50..... | IRS 12N | -3.86 | -12.91 | 8.58 ± 0.04 | 6.95 ± 0.05 | 2.83 ± 0.06 | ... | *, Cool |
| 50..... | IRS 12N | -3.86 | -12.91 | 8.48 ± 0.05 | 8.68 ± 0.23 | 2.88 ± 0.06 | 0.80 ± 0.18 | h |
| 51..... | | -3.51 | -7.21 | 10.14 ± 0.20 | ... | ... | ... | |
| 52..... | IRS 13E | -3.37 | -7.51 | 9.82 ± 0.13 | 5.71 ± 0.14 | 2.34 ± 0.14 | ... | He I |
| 52..... | IRS 13E | -3.37 | -7.51 | 9.60 ± 0.15 | ... | ... | 3.21 ± 0.16 | h |
| 53..... | IRS 3 | -2.45 | -2.01 | 11.16 ± 0.11 | ... | ... | ... | Red |
| 53..... | IRS 3 | 2.45 | -2.01 | 10.79 ± 0.07 | ... | ... | 5.52 ± 0.07 | h |
| 54..... | IRS A7 | 2.10 | 2.71 | 10.50 ± 0.05 | 6.17 ± 0.06 | 2.42 ± 0.07 | ... | |
| 55..... | IRS 29S | 1.93 | -4.91 | 10.55 ± 0.28 | 5.90 ± 0.29 | 2.57 ± 0.29 | ... | Cool |
| 56..... | IRS 29N | 1.79 | 4.41 | 9.96 ± 0.11 | ... | ... | ... | WC9 |
| 56..... | IRS 29N | 1.79 | 4.41 | 9.87 ± 0.11 | ... | ... | 2.67 ± 0.13 | b |
| 57..... | IRS 20 | -1.45 | 11.30 | 10.61 ± 0.05 | 5.89 ± 0.07 | 2.26 ± 0.07 | ... | Cool |

TABLE 1—Continued

| ID | Name | $\Delta\alpha$ (arcsec) ^a | $\Delta\delta$ (arcsec) ^a | K | $J-K$ | $H-K$ | $K-L$ | Notes |
|-----|-------------|--------------------------------------|--------------------------------------|--------------|-------------|-------------|-------------|---------------------|
| 57 | IRS 20 | -1.45 | -11.30 | 10.56 ± 0.08 | ... | ... | 0.69 ± 0.49 | ^b |
| 58 | F95 J | -1.33 | 11.60 | 10.38 ± 0.03 | 6.15 ± 0.05 | 2.40 ± 0.05 | ... | II92, Cool |
| 59 | MPE-1.0-3.5 | -1.00 | -3.76 | 11.90 ± 0.22 | ... | ... | 2.02 ± 0.46 | ^b , WC9 |
| 60 | IRS 14SW | -0.73 | -15.13 | 10.15 ± 0.04 | 6.72 ± 0.07 | 2.59 ± 0.06 | ... | Cool |
| 61 | IRS 33W | -0.68 | -9.22 | 10.87 ± 0.07 | 6.07 ± 0.11 | 2.18 ± 0.10 | ... | Cool |
| 61 | IRS 33W | -0.68 | -9.22 | 10.86 ± 0.11 | ... | ... | 1.01 ± 0.34 | ^b |
| 62 | IRS 15SW | -0.43 | 5.95 | 10.39 ± 0.04 | 5.59 ± 0.05 | 2.15 ± 0.06 | ... | He I |
| 63 | IRS A11 | -0.25 | -8.07 | 10.92 ± 0.12 | ... | ... | 2.00 ± 0.18 | ^b |
| 63 | IRS A11 | 0.25 | -8.07 | 10.87 ± 0.06 | 5.28 ± 0.07 | 2.05 ± 0.08 | ... | |
| 64 | | -0.16 | 31.53 | 10.13 ± 0.03 | 6.53 ± 0.05 | 2.51 ± 0.05 | ... | |
| 65 | IRS 16NW | -0.08 | -4.72 | 10.03 ± 0.07 | ... | ... | ... | ^b , He I |
| 65 | IRS 16NW | -0.08 | -4.72 | 10.03 ± 0.04 | 5.01 ± 0.06 | 2.01 ± 0.06 | ... | |
| 66 | IRS 7 | 0.15 | -0.24 | 6.40 ± 0.03 | 6.64 ± 0.04 | 2.42 ± 0.10 | ... | ^c , Cool |
| 66 | IRS 7 | 0.15 | -0.24 | 6.70 ± 0.10 | 7.10 ± 0.14 | 2.60 ± 0.14 | 2.15 ± 0.14 | |
| 67 | IRS 33E | 0.31 | -9.13 | 10.02 ± 0.05 | 5.57 ± 0.06 | 2.21 ± 0.07 | ... | He I |
| 67 | IRS 33E | 0.31 | -9.13 | 9.86 ± 0.06 | ... | ... | 0.73 ± 0.25 | ^b |
| 68 | IRS 14NE | 0.36 | -14.21 | 9.75 ± 0.04 | 6.80 ± 0.06 | 2.64 ± 0.06 | ... | Cool |
| 69 | | 0.39 | -34.01 | 9.79 ± 0.03 | 7.02 ± 0.08 | 2.75 ± 0.05 | ... | |
| 70 | F95 B | 0.44 | -28.15 | 9.88 ± 0.06 | 6.30 ± 0.07 | 2.49 ± 0.08 | ... | Cool |
| 71 | IRS 16SW | 0.67 | -7.15 | 9.60 ± 0.05 | 5.15 ± 0.06 | 2.00 ± 0.07 | ... | He I |
| 71 | IRS 16SW | 0.67 | -7.15 | 9.34 ± 0.10 | ... | ... | 1.30 ± 0.12 | ^b |
| 72 | F95 A | 0.82 | -36.34 | 9.05 ± 0.04 | 3.74 ± 0.05 | 1.27 ± 0.05 | ... | Cool |
| 73 | | 0.90 | -7.70 | 10.03 ± 0.07 | 5.40 ± 0.08 | 2.05 ± 0.09 | ... | |
| 74 | IRS 16C | 1.12 | -5.61 | 9.86 ± 0.05 | 5.37 ± 0.06 | 2.13 ± 0.06 | ... | He I |
| 74 | IRS 16C | 1.12 | -5.61 | 9.79 ± 0.05 | ... | ... | 1.31 ± 0.09 | ^b |
| 75 | IRS 15NE | 1.38 | 5.61 | 8.96 ± 0.04 | 6.03 ± 0.05 | 2.41 ± 0.05 | ... | He I & Cool |
| 76 | OSUF 1 | 1.38 | -12.49 | 11.40 ± 0.08 | 5.38 ± 0.11 | 2.18 ± 0.11 | ... | ^r |
| 76 | OSUF 1 | 1.38 | -12.49 | 11.31 ± 0.14 | ... | ... | ... | ^b |
| 77 | MPE 1.6 6.8 | 1.58 | -7.21 | 9.98 ± 0.06 | 6.00 ± 0.08 | 2.42 ± 0.08 | ... | WC9 |
| 77 | MPE 1.6 6.8 | 1.58 | -7.21 | 9.88 ± 0.14 | ... | ... | 2.00 ± 0.14 | ^b |
| 78 | IRS 8 | 1.88 | 23.90 | 10.49 ± 0.06 | ... | ... | ... | Red |
| 79 | | 2.01 | 42.73 | 9.73 ± 0.13 | 6.60 ± 0.13 | 2.28 ± 0.13 | ... | |
| 80 | IRS 16CC | 2.02 | 5.61 | 10.51 ± 0.11 | ... | ... | 1.85 ± 0.16 | ^b |
| 80 | IRS 16CC | 2.02 | -5.61 | 10.20 ± 0.07 | 5.36 ± 0.09 | 2.08 ± 0.09 | ... | He I |
| 81 | IRS 21 | 2.22 | -8.83 | 10.40 ± 0.05 | ... | ... | ... | Red |
| 81 | IRS 21 | 2.22 | 8.83 | 10.11 ± 0.06 | ... | ... | 3.20 ± 0.06 | ^b |
| 82 | TAM HeI | 2.59 | 11.82 | 12.05 ± 0.13 | ... | ... | ... | ^r , He I |
| 82 | TAM HeI | 2.59 | 11.82 | 12.01 ± 0.19 | ... | ... | ... | ^b |
| 83 | IRS 16NE | 2.89 | -4.90 | 9.01 ± 0.05 | 5.00 ± 0.06 | 1.93 ± 0.06 | ... | He I |
| 83 | IRS 16NE | 2.89 | -4.90 | 8.99 ± 0.05 | ... | ... | 1.44 ± 0.07 | ^b |
| 84 | | 3.08 | -17.50 | 9.88 ± 0.04 | 7.38 ± 0.08 | 3.06 ± 0.07 | ... | |
| 85 | | 3.12 | -7.23 | 11.00 ± 0.08 | 5.08 ± 0.09 | 2.02 ± 0.10 | ... | |
| 85 | | 3.12 | -7.23 | 10.95 ± 0.12 | ... | ... | 1.41 ± 0.20 | ^b |
| 86 | | 3.45 | -8.42 | 11.79 ± 0.13 | ... | ... | ... | |
| 87 | IRS A19 | 3.67 | -13.25 | 11.61 ± 0.09 | 6.94 ± 0.29 | ... | 1.85 ± 0.23 | ^b |
| 87 | IRS A19 | 3.67 | -13.25 | 11.18 ± 0.06 | ... | 2.53 ± 0.08 | ... | |
| 88 | | 5.01 | -13.32 | 10.03 ± 0.18 | 7.17 ± 0.20 | ... | ... | |
| 89 | OSU HeI | 5.35 | -3.01 | 12.36 ± 0.23 | ... | ... | ... | ^r , He I |
| 90 | | 5.40 | 28.38 | 10.11 ± 0.08 | 5.82 ± 0.09 | 1.96 ± 0.09 | ... | |
| 91 | IRS 9 | 5.42 | -12.60 | 8.53 ± 0.04 | 6.45 ± 0.05 | 2.46 ± 0.06 | ... | ^c , Cool |
| 91 | IRS 9 | 5.42 | -12.60 | 8.61 ± 0.03 | 7.33 ± 0.07 | 2.24 ± 0.04 | 1.45 ± 0.04 | ^b |
| 92 | IRS 1W | 5.42 | -5.61 | 8.66 ± 0.04 | ... | ... | 3.16 ± 0.07 | ^b |
| 92 | IRS 1W | 5.42 | -5.61 | 8.81 ± 0.04 | 6.21 ± 0.06 | 3.13 ± 0.07 | ... | ^r , Red |
| 93 | | 6.63 | -6.01 | 10.70 ± 0.13 | 5.86 ± 0.18 | ... | 2.14 ± 0.22 | ^b |
| 93 | | 6.63 | -6.01 | 10.61 ± 0.13 | ... | 2.37 ± 0.16 | ... | |
| 94 | IRS 10W | 6.91 | -0.97 | 10.27 ± 0.06 | 6.48 ± 0.08 | 3.13 ± 0.08 | ... | |
| 94 | IRS 10W | 6.91 | -0.97 | 10.22 ± 0.07 | ... | ... | 3.42 ± 0.07 | ^b |
| 95 | | 7.07 | 5.21 | 10.62 ± 0.09 | 6.04 ± 0.13 | ... | 1.78 ± 0.17 | ^b |
| 95 | | 7.07 | 5.21 | 10.46 ± 0.07 | ... | 2.56 ± 0.10 | ... | |
| 96 | IRS 1NE | 7.28 | 4.33 | 10.32 ± 0.08 | ... | ... | 1.50 ± 0.12 | ^b |
| 96 | IRS 1NE | 7.28 | 4.33 | 10.00 ± 0.07 | ... | 2.50 ± 0.09 | ... | Cool |
| 97 | IRS 1SB | 7.49 | -6.58 | 10.28 ± 0.06 | ... | ... | ... | ^b |
| 97 | IRS 1SB | 7.49 | -6.58 | 10.23 ± 0.04 | 6.66 ± 0.11 | 2.46 ± 0.06 | ... | Cool |
| 98 | IRS 10EL | 8.07 | -1.82 | 10.75 ± 0.09 | ... | ... | 4.25 ± 0.09 | ^c |
| 99 | | 8.63 | -24.83 | 9.76 ± 0.03 | 6.50 ± 0.05 | 2.45 ± 0.05 | ... | |
| 100 | | 8.80 | 3.79 | 10.38 ± 0.04 | 6.97 ± 0.08 | 3.92 ± 0.08 | ... | |
| 101 | IRS 10E | 8.95 | -2.04 | 10.36 ± 0.06 | 6.22 ± 0.07 | 2.17 ± 0.08 | ... | Cool |
| 102 | IRS 28 | 10.57 | -12.09 | 9.36 ± 0.03 | 6.94 ± 0.05 | 2.81 ± 0.05 | ... | Cool |
| 103 | OSU C2 | 10.82 | -5.03 | 10.10 ± 0.04 | 6.20 ± 0.06 | 2.35 ± 0.06 | ... | Cool |
| 104 | | 11.63 | -2.42 | 10.47 ± 0.04 | 5.93 ± 0.05 | 2.21 ± 0.05 | ... | |
| 105 | | 13.32 | -0.66 | 8.91 ± 0.03 | 6.28 ± 0.04 | 2.32 ± 0.05 | ... | |
| 106 | | 13.45 | 6.89 | 10.33 ± 0.03 | 6.27 ± 0.05 | 2.41 ± 0.05 | ... | |

TABLE 1—Continued

| ID | Name | $\Delta\alpha$ (arcsec) ^a | $\Delta\delta$ (arcsec) ^a | K | $J-K$ | $H-K$ | $K-L$ | Notes |
|----------|--------|--------------------------------------|--------------------------------------|--------------|-------------|-------------|-------|-------------------|
| 107..... | | 13.72 | 17.46 | 10.10 ± 0.03 | 6.27 ± 0.04 | 2.35 ± 0.04 | ... | |
| 108..... | IRS 19 | 14.43 | -25.74 | 8.22 ± 0.03 | 6.59 ± 0.04 | 2.61 ± 0.04 | ... | ^c Cool |
| 109..... | IRS 18 | 14.94 | -17.40 | 9.50 ± 0.03 | 6.36 ± 0.04 | 2.40 ± 0.04 | ... | |
| 110..... | | 15.55 | -28.56 | 10.07 ± 0.04 | 7.09 ± 0.07 | 2.95 ± 0.05 | ... | |
| 111..... | | 16.55 | 44.67 | 10.39 ± 0.04 | 6.48 ± 0.10 | 2.24 ± 0.06 | ... | |
| 112..... | OSU C3 | 17.09 | -11.31 | 10.73 ± 0.04 | ... | 3.06 ± 0.05 | ... | Cool |
| 113..... | | 17.69 | -0.87 | 10.01 ± 0.04 | ... | 2.59 ± 0.07 | ... | |
| 114..... | | 18.28 | 44.62 | 8.53 ± 0.04 | 5.81 ± 0.05 | 2.24 ± 0.05 | ... | ^e |
| 115..... | | 20.23 | 22.67 | 10.26 ± 0.04 | 6.14 ± 0.05 | 2.35 ± 0.05 | ... | |
| 116..... | OSU C1 | 20.61 | -8.91 | 10.64 ± 0.04 | ... | 2.53 ± 0.06 | ... | Cool |
| 117..... | | 20.67 | 24.29 | 10.40 ± 0.04 | 5.90 ± 0.05 | 2.25 ± 0.05 | ... | |
| 118..... | | 21.42 | 32.42 | 10.27 ± 0.03 | 6.04 ± 0.05 | 2.31 ± 0.04 | ... | |
| 119..... | | 23.26 | 25.08 | 10.38 ± 0.03 | 6.72 ± 0.06 | 2.59 ± 0.05 | ... | |
| 120..... | | 23.31 | 3.24 | 10.48 ± 0.03 | 7.00 ± 0.07 | 2.75 ± 0.05 | ... | |
| 121..... | | 23.45 | 17.26 | 9.52 ± 0.03 | 7.13 ± 0.04 | 2.83 ± 0.04 | ... | |
| 122..... | | 26.16 | 38.74 | 10.20 ± 0.04 | 5.67 ± 0.05 | 2.07 ± 0.05 | ... | |
| 123..... | | 28.27 | 3.63 | 10.04 ± 0.03 | 6.88 ± 0.05 | 2.70 ± 0.04 | ... | |
| 124..... | | 32.45 | 30.92 | 9.10 ± 0.03 | 5.34 ± 0.04 | 1.96 ± 0.04 | ... | |
| 125..... | | 33.66 | 43.92 | 10.46 ± 0.04 | 6.39 ± 0.07 | 2.51 ± 0.06 | ... | |
| 126..... | | 35.29 | 28.04 | 9.69 ± 0.03 | 6.86 ± 0.05 | 2.85 ± 0.05 | ... | |
| 127..... | | 35.80 | 23.53 | 10.31 ± 0.03 | 4.91 ± 0.09 | 1.84 ± 0.11 | ... | |
| 128..... | IRS 24 | 36.66 | 24.18 | 8.26 ± 0.04 | 6.36 ± 0.06 | 2.45 ± 0.05 | ... | ^c Cool |
| 129..... | | 38.80 | 39.37 | 9.38 ± 0.03 | 5.47 ± 0.04 | 2.11 ± 0.05 | ... | |
| 130..... | | 38.91 | 30.15 | 10.43 ± 0.03 | 6.10 ± 0.05 | 2.38 ± 0.05 | ... | |
| 131..... | | 40.03 | 9.35 | 8.91 ± 0.03 | 5.51 ± 0.04 | 1.90 ± 0.05 | ... | |
| 132..... | | 40.71 | 5.48 | 10.24 ± 0.03 | 6.23 ± 0.05 | 2.44 ± 0.05 | ... | |
| 133..... | | 40.72 | -29.72 | 9.20 ± 0.03 | 6.54 ± 0.04 | 2.63 ± 0.04 | ... | H92 |
| 134..... | | 40.74 | -41.92 | 10.39 ± 0.03 | 4.80 ± 0.05 | 1.66 ± 0.05 | ... | |
| 135..... | OSU C4 | 40.82 | -4.50 | 10.67 ± 0.03 | ... | 2.67 ± 0.04 | ... | Cool |
| 136..... | IRS 23 | 42.51 | 8.19 | 8.62 ± 0.03 | 6.51 ± 0.04 | 2.58 ± 0.04 | ... | ^c Cool |
| 137..... | | 43.67 | 40.36 | 10.18 ± 0.04 | 5.79 ± 0.05 | 2.17 ± 0.05 | ... | |
| 138..... | | 45.68 | 11.15 | 10.40 ± 0.04 | 6.09 ± 0.05 | 2.65 ± 0.07 | ... | H92 |
| 139..... | | 46.08 | 0.38 | 9.89 ± 0.03 | 4.88 ± 0.04 | 1.75 ± 0.04 | ... | |
| 140..... | | 46.84 | 15.82 | 9.44 ± 0.03 | 5.73 ± 0.04 | 2.16 ± 0.04 | ... | |
| 141..... | | 48.27 | 22.84 | 10.23 ± 0.03 | 5.49 ± 0.04 | 2.01 ± 0.04 | ... | |
| 142..... | | 53.16 | 25.96 | 9.91 ± 0.03 | 5.56 ± 0.04 | 2.14 ± 0.05 | ... | |
| 143..... | | 56.84 | 28.00 | 9.86 ± 0.03 | 5.11 ± 0.04 | 1.88 ± 0.05 | ... | |
| 144..... | | 56.93 | 18.83 | 10.30 ± 0.04 | 5.74 ± 0.05 | 2.15 ± 0.05 | ... | |
| 145..... | | 62.56 | 22.02 | 10.45 ± 0.03 | ... | 3.28 ± 0.05 | ... | |
| 146..... | | 65.70 | 11.53 | 10.45 ± 0.03 | 7.24 ± 0.09 | 2.89 ± 0.05 | ... | H92 |
| 147..... | | 67.47 | 15.40 | 9.83 ± 0.04 | 4.63 ± 0.05 | 1.63 ± 0.05 | ... | |

Notes—All photometry is from our primary OSIRIS data set unless otherwise noted. The OSIRIS magnitudes include both measurement and calibration uncertainties. The DS91 data include only measurement uncertainty; calibration uncertainty is not included. IRS "A" names are taken from Tamura et al. 1996. Label "B" refers to a (usually) fainter source very close to the primary source. Earlier, lower resolution data likely included both components as a single source. H92 identifies a source of similar brightness and within 2" of a variable star identified by Huller 1992. P95 refers to sources observed by Piger 1995. Cool identifies a star with CO 2.3 μ m absorption based on K -band spectra; see LRT, Sellgren et al. 1987, Krabbe et al. 1995, and Paper II. He I identifies a star with 2.06 μ m emission based on K -band spectra or narrow-band imaging; see Allen et al. 1990, Krabbe et al. 1991, 1995, Libouste et al. 1995, Blum et al. 1995a, and Tamblyn et al. 1996. Red identifies a star with a very red, nearly featureless spectrum based on K -band spectra; see Libouste et al. 1995, Blum et al. 1995a, and Krabbe et al. 1995. WC9 identifies a star with C III and C IV emission lines based on K -band spectra; see Blum et al. 1995b and Krabbe et al. 1995.

^a Offset in arcseconds from IRS 7.

^b Photometry derived from the DePoy & Sharp 1991 data set. J and H presented from DS91 data only if no value from the OSIRIS data was available (except for IRS 7, 9, and 12N; see note e below); see Appendix. The DS91 data were flux calibrated by assuming the IRS 7 magnitudes of Becklin et al. 1978 which are uncertain by less than ± 0.1 mag at each wavelength. Good average agreement between the DS91 photometry and OSIRIS photometry argues that the assumed magnitudes of IRS 7 at the time of the DS91 observations were correct, despite the variability of IRS 7 (see text).

^c K magnitude derived from narrow-band filters at 2.2 μ m; see text.

^d IRS 2 and 10B label the bright sources at K . IRS 2L and 10BJ label the nearby, but not coincident, bright sources at L . For IRS 2L and 10BJ, we give K from OSIRIS and L from DS91. IRS 10BJ has been identified as a variable star by Tamura et al. 1996 which they call IRS 10s. It may also be the OH/IR star OH 359.946 - 0.047 in the list of Lindqvist et al. 1992.

^e See discussion in text on IRS 7, 9, and 12N variability. DS91 magnitudes for IRS 7 are from Becklin et al. 1978 as adopted by DS91. Uncertainty is less than ± 0.1 mag at each wavelength. OSIRIS H magnitude for IRS 7 is from lower resolution image taken 2 months prior (1993 May 11) to the primary OSIRIS images; see text.

^f OSU He I (IRS A22) is an He I emission-line star; OSU F1 (IRS A15) is featureless, both based on unpublished K -band spectra.

^g He I emission-line star identified by Tamblyn et al. 1996 narrow-band photometry, confirmed by our unpublished K -band spectrum.